NATIONAL ADVISORY COMMITTEE FOR AERONAUTICS

TECHNICAL NOTE

No. 1536

BIAXIAL PLASTIC STRESS-STRAIN RELATIONS FOR 24S-T ALUMINUM ALLOY

By Joseph Marin, J. H. Faupel, V. L. Dutton, and M. W. Brossman

Pennsylvania State College

Washington

May 1948

NATIONAL ADVISORY COMMITTEE FOR AERONAUTICS

TECHNICAL NOTE NO. 1536

BIAXIAL PLASTIC STRESS-STRAIN RELATIONS FOR 24S-T ALUMINUM ALLOY

By Joseph Marin, J. H. Faupel, V. L. Dutton, and M. W. Brossman

SUMMARY

The object of this investigation was to determine the yield strength, ultimate strength, ductility, and plastic stress-strain relations for 24S-T aluminum alloy when subjected to biaxial stresses. Both biaxial stresses considered were tensile and the influence of various biaxial stress ratios on the mechanical properties was determined. Biaxial tensile stresses were produced in a tubular specimen by a specially designed testing machine. This testing machine applies both an axial tensile load and internal pressure to the tubular specimen, thereby producing biaxial tensile stresses in the tube wall. Strains were measured in the plastic range up to rupture by means of special electric SR-4 clip gages. Nominal stress-strain diagrams for the elastic range and true stress-strain diagrams for the plastic range were plotted for various biaxial stress ratios.

The data were interpreted by a generalized St. Venant theory in an attempt to predict the biaxial stress-strain relations in terms of the uniaxial tensile stress-strain relations. The stress-strain relations, as predicted for combined stresses by this theory agree approximately with the test results. The yield-strength values, as determined by tests, agree quite well with the distortion energy theory, and the ultimate and fracture strengths agree well with the maximum stress theory.

Stress-strain data were obtained from flat control specimens cut from the tubular specimens and compared with tension test data obtained from tubular specimens. Except for ductility values, the results show that the tension test results for these control specimens agree with the values for the longitudinal tension tests on the tubular specimens.

INTRODUCTION

Aircraft members may be subjected to stresses beyond the yield strength of the material. In many cases the stresses are not simple stresses acting in one direction, but the stresses act in several

directions; that is, the biaxial stresses often occur in place of uniaxial stresses. It is of importance, therefore, to determine the plastic stress-strain relations and the mechanical properties in aircraft materials subjected to combined stresses.

During World War II, biaxial stress plasticity studies were made on sheet aluminum alloys for the purpose of obtaining basic information which could be used to improve forming operations. It is hoped that the results given in this report also may be of value in forming problems.

In obtaining the plastic stress-strain relations to rupture for various biaxial stress ratios, information is obtained to show the influence of the biaxial stress ratio on the yield strength, ultimate strength, true fracture strength, and ductility. It is of great importance to know the influence of biaxial stresses on strength and ductility, since the factor of safety and resulting design stresses selected may be appreciably modified by considering the combined stress effect.

In this investigation stress-strain data and mechanical properties for various ratios of biaxial tensile stresses were determined for 24S-T aluminum alloy by subjecting a tubular specimen to axial tension and internal pressure. Professor K. J. DeJuhasz gave valuable suggestions on the design of the testing machine. The special testing machine and strain-measuring equipment were built by Messrs. S. S. Eckley, E. Grove, and H. Johnson. Messrs. J. H. Faupel, V. L. Dutton, and M. W. Brossman, performed the tests and computed and plotted the test data. The technical assistance given by the foregoing individuals in making possible this investigation is greatly appreciated. The testing machine was designed by Joseph Marin, who directed the project and prepared this report.

This work was conducted at The Pennsylvania State College under the sponsorship and with the financial assistance of the National Advisory Committee for Aeronautics.

SYMBOLS

A	cross-sectional area, square inches
A_o	original cross-sectional area of tension specimen, square inches
d	original internal diameter of tubular specimen, inches
d_p	internal diameter of tubular specimen in plastic range, inches

d_p	external diameter of tubular specimen in plastic range, inches
E_r	percent error in measured strains in plastic range, inches
E	Young's modulus of elasticity, psi
e_e	equivalent-offset strain for combined stresses, inches per inch
e_t	offset strain for tension, inches per inch
e_o	nominal uniaxial unit strain, inches per inch
e_{1e}, e_{2e}	longitudinal and lateral nominal strains in elastic range, respectively, inches per inch
e_1, e_2	longitudinal and lateral nominal strains in plastic range, respectively, inches per inch
F	total axial force, pounds
k	experimental constant for simple tension
k_s	transverse sensitivity constant of SR-4 gages
k_1	plasticity modulus $\left(\frac{3}{2}\frac{\epsilon}{\sigma}\right)$
L	gage length of tension specimen in plastic range, inches
L_o	original gage length of tension specimen, inches
μ	Poisson's ratio
n	strain-hardening coefficient for simple tension
p	internal pressure, psi
P	axial tension load, pounds
q	nominal reduction in area of tension specimen

q'	true reduction in area of tension specimen
t	original wall thickness of tubular specimen, inches
t_p	wall thickness of tubular specimen in plastic range, inches
x, y	principal stress ratios
σ	true stress in simple tension, psi
σ_e	equivalent uniaxial yield stress as defined by distortion energy theory, psi
σ_y	yield stress in simple tension, psi
σ_u	nominal ultimate stress in simple tension, psi
σ_r	true rupture stress in simple tension, psi
σ_1, σ_2	true longitudinal and lateral principal stresses, respectively, psi
σ_{1e}, σ_{2e}	elastic longitudinal and lateral principal stresses, respectively, psi
σ_{1y}, σ_{2y}	yield longitudinal and lateral principal stresses, respectively, psi
σ_{1u}, σ_{2u}	nominal ultimate longitudinal and lateral principal stresses, respectively, psi
σ_{1r}, σ_{2r}	true-rupture longitudinal and lateral principal stresses, respectively, psi
σ_x, σ_y	stress components, psi
$\bar{\sigma}$	significant stress, psi
τ_{xy}	shear stress component, psi
τ_1, τ_2, τ_3	principal shear stresses, psi
τ_r	true rupture stress in shear, psi
γ_1, γ_2, γ_3	principal shear strains, inches per inch

ϵ	true strain in simple tension, inches per inch
$\epsilon_1, \epsilon_2, \epsilon_3$	true principal strains, inches per inch
$\bar{\epsilon}$	significant strain, inches per inch
δ_1, δ_2	apparent recorded measured strains in longitudinal and lateral directions, respectively, inches per inch
α	stress ratio $\left(\sigma_{2e}/\sigma_{1e} \text{ or } \sigma_2/\sigma_1\right)$
β	stress ratio $\left(\sigma_3/\sigma_1\right)$

DESCRIPTION OF MATERIAL

The material tested in this investigation was a fully heat-treated aluminum alloy designated 24S-T. The material was supplied in tubular extruded form in lengths of 16 feet with an internal diameter of 2 inches and a wall thickness of 1/4 inch. The nominal chemical composition, in addition to aluminum and normal impurities, consists of 4.4 percent copper, 1.5 percent magnesium, and 0.6 percent manganese. The mechanical properties, as furnished by the manufacturer, are: tensile strength, 68,000 psi; yield strength (0.2-percent offset), 44,000 psi; modulus of elasticity, 10.6×10^6 psi; percent elongation (in 2 in.), 14 percent; and Poisson's ratio, 0.33.

Tensile control tests were made on flat specimens machined from the walls of the tubular extrusions. These tests were made to obtain more accurate values of the tensile properties and to make possible the correlation of the combined-stress test results with tensile tests on specimens of the usual type. The dimensions of these control specimens are shown in figure 1. The longitudinal direction of these specimens coincided with the longitudinal direction of the tubular extrusions from which they were cut. The tension tests were made on a 60,000-pound hydraulic machine, and strains were measured to rupture. Elastic strains were measured with SR-4 electric strain gages and plastic strains were measured by using clip gages as described for the combined-stress tests. Four specimens were selected from each of the three 16-foot tube lengths used for the combined-stress tests. Figure 2 shows the nominal stress-strain diagrams for the 12 specimens tested. The values of moduli of elasticity and tensile yield strengths based on 0.2-percent offset, as obtained from figure 2, are given in table 1. The nominal values of tensile ultimate strength and percent elongation based on the original specimen dimensions are also given in table 1.

Figure 3 shows the true stress-strain diagrams for the tension control specimens based on the changing dimensions; the values of stress and strain used are defined by equations (A10) and (A8) in appendix A. Tension tests on many metals (references 1 and 2) show that in the plastic range there is an approximate linear relation between the true stress σ and true strain ϵ when they are plotted on logarithmic paper; that is, the relation $\sigma = k\epsilon^n$ is a good approximation. In order to determine the constants k and n in this equation, the true stress-strain data shown in figure 3 were plotted on logarithmic graph paper, as shown in figure 4. The values of the material constants k and n, as obtained from figure 4, are given in table 1. The values of these constants were obtained in order to correlate the plastic stress-strain data on tension specimens of usual dimensions with the simple tension test data of tubular specimens.

TEST PROCEDURE

Test Specimen

The biaxial-stress test specimens were machined from tubular sections having an inside diameter of 2 inches and wall thickness of 1/4 inch. The dimensions of the machined specimen are shown in figure 5. The specimen used had an over-all length of 16 inches, with an intermediate length of 11 inches of reduced wall thickness equal to 0.100 ± 0.002 inch. The internal surface was left in the extruded form. The wall thickness of the tubular specimens was measured with the apparatus shown in figure 6. This apparatus is similar to a device developed by the National Bureau of Standards for this purpose. With this equipment the reading on a 0.0001-inch dial is recorded when the dial plunger is in contact with the protrusion P on the rod, as shown in figure 6. The tubular specimen is then supported on the rod protrusion by placing the specimen over the rod. With the specimen in this position a reading on the dial indicator is recorded. The difference in the dial readings is then a measure of the wall thickness. Wall-thickness values were in this way measured for six positions around the circumference and at five equal intervals along the tube length. The ratio of wall thickness to diameter of the specimen was 0.05, so that the biaxial stresses throughout the wall were essentially uniform. The diameter-length ratio of the specimen was about 0.18, thereby providing a sufficiently long section of the specimen free from the bending stresses produced by end restraints.

Testing Machine

A special testing machine was designed and built for applying internal pressures and axial tensile loads to the tubular specimens. Figure 7 shows a schematic drawing of the testing machine, and figures 8 and 9 are photographs showing, respectively, the equipment for applying the axial load and the internal pressure. The axial tensile load is applied to the specimen S by means of a direct-current motor M, a speed-reducing unit U, a vertical pulling rod R, and a lever L. The axial load is measured by a dynamometer D. The lever L transmits the load to the specimen through spherical seats S' to insure axiality of loading. The fulcrum F of the lever and the ends of the lever are provided with bearings. The pulling rod R was provided with a spherical seat and a universal joint to eliminate bending.

The internal pressure was applied by an injection pump unit P (figs. 7 and 9). The oil used to apply the internal pressure was a "hydraulic pressurizing oil" of 154 S.S.U. viscosity at 100° F and had a pour point below -40° F. The oil was supplied by the pump P through a high-pressure pipe line to the lower pulling head H and into the specimen S. The rate of pressure application was controlled by the rheostat of a motor-generator set and by means of a release valve which discharged surplus oil into the oil supply reservoir. The oil pressure was measured by 10,000-psi, 5000-psi, and 2000-psi U. S. Bourdon gages G. Three pressure gages were used to obtain the necessary accuracy of pressure measurement during various stages of loading. The low-pressure gage was located at the end of the pressure line so that it could be shut off by a check valve when the pressure exceeded 2000 psi. A check valve was also provided between the 5000- and 10,000-psi gages to shut off the 5000-psi gage when pressures exceeding 5000 psi were applied.

The axiality of the load was checked by using three SR-4 electric strain gages cemented at 120° intervals around the circumference of a tubular specimen. The plate supporting the upper spherical seat was then shifted until the strain readings on the three strain gages were equal. The machine was calibrated for axial loading by inserting a calibrated rod with SR-4 gages in place of the specimen S and recording the readings on the dynamometer D. The axial load on the specimen was measured within 100 pounds. The pressure gages were calibrated before testing and were found to have a maximum error of about 2 percent.

Method of Measuring Strains

The elastic strains were measured over a gage length of 13/16 inch by means of SR-4 electric strain gages. Three longitudinal and three

transverse elastic gages (elastic gages refer to gages used to measure elastic strains) were located at intervals of 120° around the circumference and at three locations along the length of the specimen, as shown by the developed view of the specimen in figure 10. The strain gages were cemented to the specimens in accordance with the procedure prescribed by their manufacturer. Figure 11 is a photograph of a tubular specimen with the elastic SR-4 gages. In order to compensate for changes in specimen dimensions due to temperature changes, the elastic gages were connected to an unstressed dummy specimen of the same material as the specimen. The wiring diagram used for measuring the strains is given in figure 12, and figure 13 shows the strain-measuring apparatus. The gages are connected through a switch box B so that each gage can be successively switched into the circuit connected with the strain indicator I, which in turn records the strain directly in microinches per inch.

The SR-4 gages have a maximum range of about 0.015 inch per inch so that they could not be used to measure the plastic strains covering the entire plastic range of the material. It was necessary, therefore, to develop special plastic strain-measuring equipment for this purpose. Clip-type gages were used to measure the longitudinal and lateral plastic strains, as shown in figures 14 and 15. A clip gage consists of a channel-shaped phosphor-bronze strip to which SR-4 electric strain gages are cemented on the upper and lower surfaces of the clip-gage bridge (fig. 14). By means of this arrangement an additional temperature-compensating gage is not required and increased sensitivity is obtained. By means of these clip gages a large strain at the pivot points of the clip is reduced to a small measurable strain at the bridge of the clip. The attachment of the clip gages to the tubular specimen introduced a problem, since it was considered inadvisable to solder lugs onto the specimens for attaching the clip gages. For this reason, special clip-gage attachments were devised, as shown in figures 14 and 13. The longitudinal and lateral clip gages were capable of measuring strains to 0.00005 inch per inch. The longitudinal clip gages were calibrated by using a vernier scale, as shown in figure 16. The calibration was made by taking simultaneous readings on the micrometer and the SR-4 strain indicator. The longitudinal clip gages had a gage length of about 2 inches. The lateral clip gages were calibrated by the stepped-tube device shown in figure 17. The stepped tube consists of an accurately machined tube with lengths of various diameters. By recording the reading of the SR-4 indicator for corresponding accurately known diameters of the tube, the calibration of the lateral strain gages was made possible.

The longitudinal clip gages were applied to the specimen in a prestrained condition, since tensile stresses in the specimen reduced the strain on the gage. The lateral clip gages were applied with various amounts of prestrain, the amount depending upon the biaxial state of

stress under test; that is, various amounts of prestrain were necessary because in some tests the specimens reduced in diameter, whereas in others there was an increase in diameter. Final strains at rupture were measured to 0.01 inch by means of dividers and a scale.

Method of Testing

The elastic SR-4 clip gages were first attached to a tubular specimen and connected to the switching box and strain indicator, as shown in figure 13. Oil was then pumped through the specimen to remove any air that might be trapped in the specimen. The discharge outlet in the pulling head of the testing machine was then sealed and a protection shield was placed over the specimen end of the testing machine. Strain readings for the six elastic and six plastic strain gages corresponding to zero loading were then recorded. The specimen was loaded to predetermined values of axial load and internal pressure to produce a given principal stress ratio in the specimen. Strain readings were recorded for selected load intervals to rupture, with the stress ratio maintained essentially constant. Fracture loads were recorded also, but because of the high rate of deformation it was impossible to obtain strain readings immediately preceding fracture. Strain readings for each load increment required less than 1 minute, and the time of testing averaged about 1 hour.

TEST RESULTS

Conventional Stress-Strain Results

The conventional stress-strain diagrams are shown in figures 18 and 19. These diagrams represent the nominal stress-strain data and are based on the original dimensions and gage length. The strain values were obtained from the SR-4 gages cemented to the specimens. In figure 18, α refers to the stress ratio σ_{2e}/σ_{1e}, where σ_{1e} is the longitudinal stress and σ_{2e} is the lateral, transverse, or circumferential stress; that is, a value of $\frac{\sigma_{2e}}{\sigma_{1e}} = 0$ represents a tubular specimen subjected only to axial tension without internal pressure. Strain values in figures 18 and 19 are plotted for only the strains nearest the point of rupture of the specimen. At least three specimens were tested for each principal stress ratio. The equation for the nominal longitudinal stresses plotted in figure 18 is

$$\sigma_{1e} = \frac{\frac{p\pi d^2}{4} + P}{\frac{\pi}{4}\left[(d + 2t)^2 - d^2\right]} = \frac{pd^2 + 4P/\pi}{4t(d + t)} \tag{1}$$

The values of the nominal lateral stresses plotted in figure 19 were determined by the equation for a thick-walled tube, since the use of the formulas for a thin-walled tube produces an error of about 5 percent in the stresses; that is, the maximum value of the lateral principal stresses is (reference 3)

$$\sigma_{2e} = \frac{pd}{2t}\left[\frac{1 + 2\frac{t}{d} + 2\left(\frac{t}{d}\right)^2}{1 + \frac{t}{d}}\right] \tag{2}$$

The value of $\frac{t}{d} = 0.05$ for the tubes tested, so that the circumferential stress is defined approximately by

$$\sigma_{2e} = 1.05\,\frac{pd}{2t} \tag{3}$$

Since $\sigma_{2e} = pd/2t$ is the lateral stress for a thin-walled tube, the error produced by neglecting the variation in stress throughout the wall is 5 percent.

The nominal conventional strains were determined from the readings from the SR-4 indicator and the original gage length of the specimen. For some strain readings it was necessary to correct the readings for the lateral sensitivity and for the "combined-stress effect," since the calibration constant supplied by the manufacturer is based on a simple tension calibration on a steel specimen with a Poisson's ratio of 0.285. Equations for calculating the strains in terms of the apparent measured strains corrected for the combined-stress effect and Poisson's ratio were developed by Baumberger (reference 4). The application of these equations is given in appendix B. The straight dashed lines in figures 18 and 19

correspond to the stress-strain relations based on the elastic equations for biaxial stresses, if a modulus of elasticity of 10.3×10^6 psi is used.

The yield-strength values for axial tension ($\alpha = 0$) were determined by using an offset strain of 0.002 inch per inch, as indicated in figure 18. For the combined-stress tests an equivalent offset was used, as proposed by Marin (references 5 and 6). The equivalent-offset strain is a strain value corresponding to the uniaxial strain offset of 0.002 inch per inch but providing for the biaxial state of stress. The value of the equivalent-offset strain in terms of the uniaxial offset strain is

$$e_e = \frac{\sigma_y}{E}\left(1 - \frac{1 - \mu\alpha}{\sqrt{1 - \alpha + \alpha^2}}\right) + e_t \qquad (4)$$

where

σ_y yield strength in simple tension, psi

e_t offset strain for tension (0.0002 in./in. for test results reported herein)

e_e equivalent-offset strain for a particular stress ratio

Equation (4) determines the offset strains used in figures 18 and 19 to determine the yield-stress values. Table 2 gives the values of these yield stresses for each of the biaxial stress ratios. A comparison of the biaxial with the uniaxial yield strengths, based on the tensile yield strength as determined in the longitudinal direction, is shown by the last two columns of table 2. The values in these columns represent the stress ratios $x = \sigma_{1y}/\sigma_y$ and $y = \sigma_{2y}/\sigma_y$. For a particular stress ratio, when either x or y is greater than 1, then the yield strength for the stress ratio is greater than the uniaxial longitudinal tensile yield strength.

Plastic Stress-Strain Results

The stress-strain diagrams for the plastic range are shown in figures 20 and 21. These diagrams represent true stress-strain values based on changing gage lengths and dimensions of specimens in the plastic

range. As in figures 18 and 19, the data in figures 20 and 21 are plotted for only the strains nearest the point of rupture. For each principal stress ratio at least three specimens were tested.

The true plastic strains were determined by clip gages and from the readings of the SR-4 indicator. The conversion of the readings of the SR-4 indicator to unit plastic strains was made as follows: (1) Let w_1 equal a given strain reading in inches given by the calibrating device (stepped tube or vernier scale) and x_1 equal the strain reading on the SR-4 indicator corresponding to the strain w on the calibrating device. Then w_1/x_1 equals the strain in inches per division on the SR-4 indicator. (2) Let y_1 equal the gage length for the clip gage in inches. Then w_1/x_1y_1 equals the strain in inches per inch per division on the SR-4 indicator. (3) Let z_1 equal a given strain reading on the SR-4 indicator as measured for a tubular specimen under test. Then the unit strain on the specimen in inches per inch is

$$e^1 = \frac{w_1}{x_1 y_1} z_1 \tag{5}$$

The unit plastic strain, as determined by equation (5), is the nominal strain based on the original gage length. Appendix A shows that the true strain ϵ in terms of the nominal strain e' is given by the equation

$$\epsilon = \log_e(1 + e') \tag{6}$$

If e_1 and e_2 are the nominal longitudinal and lateral strains, respectively, as determined by equation (5), then the true strains are

$$\left.\begin{aligned} \epsilon_1 &= \log_e(1 + e_1) \\ \epsilon_2 &= \log_e(1 + e_2) \end{aligned}\right\} \tag{7}$$

The true strains, as defined by equation (7), are plotted in figures 20 and 21.

The stresses for the plastic range were determined by basing them on the varying dimensions, since, for the higher plastic strain values, the changes in dimensions become appreciable. The true longitudinal stress can be expressed by equation (1) for the nominal stress provided that the thickness t and diameter d are replaced by their true values. That is, the true longitudinal stress is

$$\sigma_1 = \frac{pd_p^2 + 4P/\pi}{4t_p(d_p + t_p)} \tag{8}$$

The determination of the wall thickness t_p and diameter d_p is given in appendix C. Appendix C shows that the wall thickness t_p is approximately

$$t_p = \frac{t}{1 + e_1 + e_2} \tag{9}$$

where t is the original wall thickness and e_1 and e_2 are the nominal strains in the longitudinal and lateral directions, respectively. The internal diameter d_p is shown in appendix C to be

$$d_p = (d + 2t)(1 + e_2) - 2t_p \tag{10}$$

where t_p is the new wall thickness as given by equation (9). Equation (8) can now be used to determine the longitudinal stresses since the dimensions t_p and d_p can be found by equations (9) and (10). The true lateral

stresses were calculated by using the stress formula for a thin-walled tube, namely,

$$\sigma_2 = \frac{pd_p}{2t_p} \tag{11}$$

An analysis of the stress distribution for a thick-walled tube subjected to plastic flow shows that, for the ratio of wall thickness to diameter of 1:20 used in these tests, a small amount of plastic flow yields essentially a uniformly distributed lateral stress. This is also indicated by the fact that for the elastic range the correction produced by a consideration of the thick-walled-cylinder theory produces only a 5-percent error (equation (3)). The values of the diameter d_p and wall thickness t_p used in equation (11) were determined by equations (9) and (10).

The true stress-strain diagrams plotted in figures 20 and 21 are based on stresses and strains as calculated by equations (7) to (10). In order to determine the fracture points shown in figures 20 and 21, the measured true strains at rupture were corrected for the elastic strains corresponding to the stresses just prior to rupture. This correction appears to be justified since the remaining strains plotted include an elastic strain.

On the basis of the data plotted in figures 20 and 21, tables 3 to 6 were prepared. These tables show, for the various principal stress ratios, the nominal values of the ultimate stresses, percent elongation, and the true fracture stresses and true strains at fracture. These tables also give a comparison of the mechanical properties for the various ratios of biaxial stresses with the value for uniaxial longitudinal tension. Figure 22 shows the typical types of fracture for the various stress ratios considered.

ANALYSIS AND DISCUSSION

Biaxial Yield Strength

The difference in uniaxial tensile yield-strength values in the longitudinal and lateral directions, as given in table 2 for stress ratios of ∞ and 0, makes it difficult to compare the actual yield-strength values for various stress ratios with values predicted by the

available theories of failure. The difficulty is present since the various theories of failure available assume equal tensile yield strengths in the directions of the two biaxial stresses; that is, the theories assume an isotropic and homogeneous material. Figure 23(a) gives a comparison of the yield strengths for various biaxial stresses with the stress, shear, and distortion energy theories of failure (references 5 and 6). The comparison shown in figure 23(a) is based on the uniaxial tensile strength in the longitudinal direction. In figure 23(a) the stresses are considered to be biaxial and the radial stress is neglected. Figure 23(a) shows that, except for the influence of the directional properties of the tubes, the distortion energy theory is a good approximation.

Figure 23(b) gives a comparison between the distortion energy theory and the test results with the radial stress included. This comparison is made by representing the equivalent uniaxial stress

$$\sigma_e = \sqrt{\sigma_1^2 + \sigma_2^2 + \sigma_3^2 - \sigma_1\sigma_2 - \sigma_2\sigma_3 - \sigma_3\sigma_1}$$

defined by equation (A23) as a ratio of the uniaxial tensile yield strength σ_y for the various biaxial stress ratios; that is, in figure 23(b), if the distortion theory applies, the ratio σ_e/σ_y should be 1.0 as indicated. A consideration of the three-dimensional stress effect (fig. 23(b)) shows that the distortion energy theory gives a good approximation to the test results.

Plastic Stress-Strain Results

A theory called the generalized St. Venant theory has been proposed. With this theory it is possible to predict the true stress-strain relation under combined stresses in terms of true stress-strain relations in simple tension. The theory defines a stress and strain, called the significant stress and strain (references 7 to 14), as a function of the principal true stresses and strains. These quantities are also referred to as the "effective stress-strain" and "octahedral shear stress-strain relation" in various reports. The values of the significant stress and strain are derived in appendix A and are shown to be, respectively,

$$\bar{\sigma} = \sqrt{\frac{1}{2}\left[(\sigma_1 - \sigma_2)^2 + (\sigma_2 + p)^2 + (\sigma_1 + p)^2\right]} \tag{12}$$

$$\bar{\epsilon} = \sqrt{\frac{4}{3}\left(\epsilon_1^2 + \epsilon_1\epsilon_2 + \epsilon_2^2\right)} \tag{13}$$

where ϵ_1 and ϵ_2 are the true longitudinal and lateral strains, respectively.

Values of the significant stress and strain, as given by equations (12) and (13), are plotted in figure 24 for each specimen and stress ratio. By the generalized St. Venant theory the significant stress-strain relations should all agree and coincide with the uniaxial tensile true stress-strain relation. Figure 25 shows the average curve for each principal stress ratio as obtained from figure 24 but plotted with the same origin. The uniaxial tensile true stress-strain diagram is also shown in figure 25 for purposes of comparison. It appears from figure 25 that the generalized St. Venant theory, together with the uniaxial true stress-strain relation, may be used to define approximately the true stress-strain relation for 24S-T aluminum alloy subjected to biaxial tensile stresses.

Biaxial Ultimate Strength

Table 3 gives values of the nominal ultimate stresses for various principal stress ratios based on the original dimensions of the specimen. Figure 26 gives a comparison between the biaxial ultimate strengths and the values from the stress theory of failure. Figure 26 shows that the maximum stress theory is a good approximation since average test values are within 4 percent of the theoretical values defined by this theory.

Biaxial Fracture Strengths

Table 4 gives values of the true fracture strengths, and figure 27 gives a comparison of these stresses with values predicted by the stress theory of failure. Figure 27 shows that the maximum stress theory is a good approximation. Except for one stress ratio, the average test results agree with the theory within 3 percent.

Ductility

Values of the measured nominal and true ductilities are given in table 5 for the direction of the maximum stress. A comparison of the ductilities for biaxial tensile stresses with uniaxial values shows that there is an appreciable reduction in ductility. A reduction in ductility for biaxial tensile stress is also predicted by the generalized St. Venant Theory (equation (A46)). Theoretical values of true ductility, as determined by equation (A46), were calculated. These values do not agree with the observed values. Possible reasons for this discrepancy are the presence of a nonuniform state of stress at the necked-down section of the specimen, the observation of an average rather than a local strain by using a 2-inch gage length, or the inadequacy of the theory. The foregoing reasons may also explain the reason that predicted strains at points of instability, as determined by equations (A56) and (A61), give unreasonable values.

Control Tension Tests

Table 6 gives the mechanical properties of the tension control specimens and the uniaxial tension properties as obtained from tests of the tubular specimens. A comparison of the nominal ultimate stresses and the true fracture stress values for the three types of tension test shown in table 6 shows that the values for the tension control specimens fall between the values for the longitudinal and lateral tensile strength values of the tubular specimens. The true ductility in the longitudinal direction of the tubes was found to be somewhat greater than the values for the other tension tests. The true stress-strain results obtained from the uniaxial tension tests of the tubes were plotted logarithmically as shown in figure 28, and the values of k and n obtained from figure 28 are given in table 6. A comparison of the values of k and n for the three types of tension test shows that there is little difference between the values of these constants.

CONCLUSIONS

For the 24S-T aluminum alloy tested, the following conclusions can be made:

1. The yield strengths for biaxial tension may be predicted approximately by the distortion energy theory.

2. The values of the nominal biaxial ultimate stresses for biaxial tension agree well with values based on the maximum stress theory.

3. The values of the true biaxial fracture stresses for biaxial tension agree well with values based on the maximum stress theory.

4. There is a decrease in nominal and true ductility for biaxial tension compared with uniaxial tension. However, the test values do not agree with the theoretical values based on the generalized St. Venant Theory.

5. The generalized St. Venant theory can be used to predict approximately biaxial stress-strain relations in the plastic range by using the stress-strain relations in simple tension.

The Pennsylvania State College
State College, Pa., March 17, 1947

APPENDIX A

STRESS-STRAIN PLASTICITY RELATIONS FOR COMBINED STRESSES

The object of the following analysis is to present the currently accepted theory used for predicting the stress-strain relations for combined stresses in the plastic range. In developing this analysis the following relations are determined:

1. True stress-strain relation for simple tension in the plastic range
2. The relation defining the beginning of necking for simple tension
3. The stress relation defining the beginning of yielding for combined stresses
4. The stress-strain relation for combined stresses in the plastic range
5. The strain equations for combined stresses in the plastic range
6. Fracture-strength relations for combined stresses
7. Ductility relations for combined stresses
8. Stress and strain values at beginning of necking for combined stresses

The yield strength, rupture strength, and ductility for combined stresses are determined by use of the true stress-strain relation in simple tension. In addition, the plastic stress-strain relations under combined stresses are determined by use of the true stress-strain relation in simple tension.

True Stress-Strain Relation for Simple Tension in the Plastic Range

Figure 29 shows a tension test bar of uniform cross section with an original gage length L_o and cross-sectional area A_o. When a uniaxial tension load P is applied there is a change in gage length or strain ΔL_o and a change in cross-sectional area ΔA_o. If the load remains

in the elastic range the strain and reduction in area are defined, respectively, by

$$e_o = \frac{\Delta L_o}{L_o} \tag{A1}$$

and

$$q = \frac{\Delta A_o}{A_o} \tag{A2}$$

That is, e_o and q are the axial strain and reduction in area, respectively, as usually defined.

For large deformations which occur in the plastic range beyond the yield-stress value, the quantities ΔL_o and ΔA_o become relatively large compared with the values L_o and A_o. For large strains it is then necessary to correct equations (A1) and (A2) to include the influence of a changing gage length and cross-sectional area. If for a load P the gage length becomes L and the cross-sectional area becomes A, then the true strain ϵ and true reduction in area q^1 are

$$\epsilon = \int_{L_o}^{L} \frac{dL}{L} = \log_e \frac{L}{L_o} \tag{A3}$$

and

$$q^1 = - \int_{A_o}^{A} \frac{dA}{A} = \log_e \frac{A_o}{A} \tag{A4}$$

Equations (A3) and (A4) define the true strain and true reduction in area, respectively, as distinguished from equations (A1) and (A2), which define the nominal strain and reduction in area. For elastic strains the values of e_o and ϵ and q and q^1 are essentially equal.

In the plastic range, for most ductile engineering materials, the volume remains constant. That is,

$$A_o L_o = AL$$

or

$$\frac{A_o}{A} = \frac{L}{L_o} \tag{A5}$$

On placing the value of A_o/A from equation (A5) in equation (A3), the right-hand side of equation (A3) is the same as the right-hand side of equation (A4), or,

$$\epsilon = q^1 \tag{A6}$$

Equation (A6) shows that in the plastic range the true strain ϵ equals the true reduction in area q^1.

The true strain can be related to the nominal strain by noting that in equation (A1)

$$e_o = \frac{\Delta L_o}{L_o} = \frac{L - L_o}{L_o} = \frac{L}{L_o} - 1$$

or

$$\frac{L}{L_o} = 1 + e_o \tag{A7}$$

Placing the value of L/L_o from equation (A7) in equation (A3),

$$\epsilon = \log_e (1 + e_o) \tag{A8}$$

The true reduction in area q^1 can be related to the nominal reduction in area q by noting that in equation (A2)

$$q = \frac{A_o - A}{A_o} = 1 - \frac{A}{A_o}$$

or

$$\frac{A}{A_o} = 1 - q \tag{A9}$$

Placing the value of A/A_o from equation (A9) in equation (A4) yields

$$q^1 = -\log_e(1 - q)$$

The relation given by equation (A6), namely, that the true axial strain is equal to the true reduction in area, has led to an improved method of determining the true stress-strain relation in simple tension since it is possible by simple lateral measurements on the specimen during the test to determine changes in cross-sectional dimensions or the true reduction in area q^1.

By obtaining the cross-sectional dimensions of a tensile specimen at various intervals of load to rupture, the true stress $\sigma = \frac{P}{A}$ and the true strain $\epsilon \doteq q^1 = \log_e \frac{A_o}{A}$ can be determined and a true stress-strain relation can be plotted. For flat specimens it is more convenient to measure the axial strains in place of the change in cross-sectional dimensions. In this case the true strain is given by equation (A3) and the true stress is given by equations (A5) and (A7) as

$$\sigma = \frac{P}{A} = \frac{P}{A_o}\frac{L}{L_o} = \frac{P}{A_o}(1 + e_o) \tag{A10}$$

Many tests (references 1 and 2) of ductile metals show that when the true stress and true strain are plotted on logarithmic paper the points

fall approximately on a straight line (fig. 30); that is, the true stress-strain relation for simple tension may be assumed as given by

$$\sigma = k\epsilon^n \tag{A11}$$

where k and n are experimental constants and n is called the strain hardening coefficient.

For some ductile materials the true stress-strain data depart slightly from a straight line at the lower and upper stress values when plotted on logarithmic paper. Corrections (references 15 and 16) to the stress and strain values have been proposed to compensate for these discrepancies. These corrections include the adjustment of the strain values to exclude the elastic strains and the correction for the stresses at loads near rupture due to the necking-down of the specimen.

Relation Defining Beginning of Necking for Simple Tension

The unstable condition of plastic deformation which occurs just prior to necking-down in a tension specimen is usually observed in a tension test; that is, the load in a tension test increases at a decreasing rate to a maximum value and then decreases until fracture occurs. At the maximum load the deformation becomes localized and the specimen necks down. Two opposing influences are present in the simple tension specimen. One is the influence of strain hardening, which tends to increase the load-carrying capacity of the specimen. Opposing this straightening effect is the decrease in the cross-sectional area of the specimen due to the elongation of the specimen. At beginning of necking the rate of increase of load-carrying capacity due to work hardening becomes less than the rate of decrease of load-carrying capacity produced by the decreasing cross section. This point of maximum load is defined by the condition $dP = 0$, that is, when there is no change in the load P. The point at which this instability occurs can be determined by the following analysis: If P is the tensile load, σ is the stress, and A is the area, then

$$P = A\sigma \tag{A12}$$

By equations (A4) and (A6),

$$\left.\begin{aligned} \epsilon &= \log_e \frac{A_o}{A} \\ \text{or} \\ A &= A_o e^{-\epsilon} \end{aligned}\right\} \tag{A13}$$

From equations (A12) and (A13),

$$P = A_o e^{-\epsilon} \sigma \tag{A14}$$

Since P is a function of both stress σ and strain ϵ,

$$dP = \frac{\partial P}{\partial \sigma} d\sigma + \frac{\partial P}{\partial \epsilon} d\epsilon \tag{A15}$$

From equation (A14),

$$\frac{\partial P}{\partial \sigma} = A_o e^{-\epsilon}$$

and

$$\frac{\partial P}{\partial \epsilon} = - A_o \sigma e^{-\epsilon}$$

Placing these values of $\frac{\partial P}{\partial \sigma}$ and $\frac{\partial P}{\partial \epsilon}$ in equation (A15) results in

$$dP = (A_o e^{-\epsilon})(d\sigma - \sigma d\epsilon) \tag{A16}$$

The beginning of necking is defined by placing $dP = 0$ in equation (A16). Then since $A_o e^{-\epsilon}$ is not zero, $d\sigma - \sigma d\epsilon = 0$, or

$$\frac{d\sigma}{d\epsilon} = \sigma \tag{A17}$$

that is, necking or instability occurs at the load corresponding to the point where the slope of the true stress-strain curve equals numerically the stress for that point (fig. 31). This point A can be located on

the true stress-strain curve graphically. That is, since the slope at $A = \frac{d\sigma}{d\epsilon} = \frac{\overline{AB}}{\overline{BC}}$ and $\overline{AB} = \sigma$, if $\overline{BC}$ is made equal to 1 inch per inch, the point A defines the condition given by equation (A17). It is more convenient, however, to define the point A in terms of the strain. In order to do this, the value of the stress as given by equation (A11) is substituted in equation (A17). Then

$$nk\epsilon^{n-1} = k\epsilon^{n}$$

or (A18)

$$\epsilon = n$$

By equation (A18) the strain at the limit of uniform extension or beginning of necking is given by the value of the strain hardening exponent n; that is, in figure 31 $\overline{OB} = n$ defines the point A.

Stress Relation Defining Beginning of Yielding for Combined Stresses

For ductile metals subjected to biaxial stresses, as shown in figure 32(a), tests show that the stress relation defining the beginning of yielding is approximately defined by the distortion or shear energy theory (references 5 and 6). That is,

$$\sigma_x^2 - \sigma_x\sigma_y + \sigma_y^2 + 3\tau_{xy}^2 = \sigma_y^2 \qquad (A19)$$

where σ_x, σ_y, and τ_{xy} are the combined-stress components as shown in figure 32(a) and σ_y is the yield stress for simple tension. In terms of the principal stresses, as shown in figure 32(b), equation (A19) becomes

$$\sigma_1^2 - \sigma_1\sigma_2 + \sigma_2^2 = \sigma_y^2 \qquad (A20)$$

That is, if σ_1 is the greater of the two principal stresses σ_1 and σ_2, then for a given value of σ_2 the value of σ_1 determined by

equation (A20) represents the value of σ_1 at which yielding occurs under a biaxial state of stress. If equation (A20) is divided by σ_y^2, it becomes

$$x^2 - xy + y^2 = 1 \tag{A21}$$

where x and y are the stress ratios $x = \sigma_1/\sigma_y$ and $y = \sigma_2/\sigma_y$. Equation (A21) is represented graphically by the ellipse in figure 33. Points inside this ellipse represent stress values below yielding, and a point on the ellipse represents stress values at which yielding begins.

Determination of Yield-Stress Value Based on Combined-Stress Test Data

In a combined-stress test such as a tube subjected to internal pressure and axial loading, the nominal strains are measured in the direction of the maximum principal stress and a stress-strain diagram $\sigma_1 - \epsilon_1$ is plotted as shown in figure 34. In order to define the yield-stress value for σ_1, several methods have been used. A rational approximate method which correlates the determination of the yield stress under combined stresses to the ASTM offset yield stress for simple tension is based on the determination of an equivalent-offset strain e_e for combined stresses. That is, an offset strain e_e (fig. 34(a)) which is equivalent to the offset strain e_t for simple tension is determined. The value of this offset strain has been shown to be (references 5 and 6)

$$e_e = \frac{\sigma_y}{E}\left(1 - \frac{1 - \mu\alpha}{\sqrt{1 - \alpha + \alpha^2}}\right) + e_t \tag{A22}$$

where

E	modulus of elasticity in simple tension
α	principal stress ratio $\left(\sigma_2/\sigma_1\right)$
e_t	offset strain value for defining yield stress in simple tension

The procedure to be used in applying equation (A22) is as follows. For simple tension, as shown in figure 34(b), the yield stress is determined on the basis of the offset strain ϵ_t in the usual manner as specified by the ASTM standards. By equation (A22), for a given stress ratio α, corresponding to the combined-stress test considered, the value of e_e is determined. With this value of e_e the value of the yield stress σ_{1y} is obtained as shown in figure 34(a). The experimental value σ_{1y} may then be compared with the theoretically predicted value as given by equation (A20).

For triaxial stresses defined by three principal stresses σ_1, σ_2, and σ_3, as shown in figure 35, beginning of yielding by the distortion energy theory is given by the equation

$$(\sigma_1 - \sigma_2)^2 + (\sigma_2 - \sigma_3)^2 + (\sigma_3 - \sigma_1)^2 = 2\sigma_y^2 \qquad \text{(A23)}$$

that is, if σ_1 is the largest of the principal stresses, then the value of σ_1, as determined by equation (A23) for particular values of σ_2 and σ_3, represents the value of σ_1 for beginning of yielding.

Stress-Strain Relation for Combined Stresses in the Plastic Range

A generalized St. Venant theory which predicts stress-strain relations for combined stresses in the plastic range has been proposed. These stress-strain relations are determined on the basis of the following assumptions:

(1) The directions of the principal strains ϵ_1, ϵ_2, and ϵ_3 coincide with the directions of the principal stresses σ_1, σ_2, and σ_3.

(2) The volume remains constant in the plastic range. For constancy of volume or no change in volume,

$$\epsilon_1 + \epsilon_2 + \epsilon_3 = 0 \qquad \text{(A24)}$$

(3) The ratios of the three principal shear strains to the principal shear stresses are equal and equal to a quantity k_1 determined by the tension test. The principal shear stresses and strains can be shown to be, respectively,

$$\left.\begin{aligned} \tau_3 &= \frac{\sigma_1 - \sigma_2}{2} \\ \tau_2 &= \frac{\sigma_3 - \sigma_1}{2} \\ \tau_1 &= \frac{\sigma_2 - \sigma_3}{2} \end{aligned}\right\} \tag{A25}$$

and

$$\left.\begin{aligned} \gamma_3 &= \epsilon_1 - \epsilon_2 \\ \gamma_2 &= \epsilon_3 - \epsilon_1 \\ \gamma_1 &= \epsilon_2 - \epsilon_3 \end{aligned}\right\} \tag{A26}$$

For the shear stresses to be proportional to the shear strains,

$$\frac{\gamma_1}{\tau_1} = \frac{\gamma_2}{\tau_2} = \frac{\gamma_3}{\tau_3} = 2k_1 \tag{A27}$$

Placing the values of the shear stresses and strains from equations (A25) and (A26) in equation (A27) gives

$$\frac{\epsilon_1 - \epsilon_2}{\sigma_1 - \sigma_2} = \frac{\epsilon_2 - \epsilon_3}{\sigma_2 - \sigma_3} = \frac{\epsilon_3 - \epsilon_1}{\sigma_3 - \sigma_1} = k_1 \tag{A28}$$

Solving equations (A24) and (A28) simultaneously for ϵ_1, ϵ_2, and ϵ_3 yields

$$\left.\begin{aligned}
\epsilon_1 &= \frac{k_1}{3}\left[(\sigma_1 - \sigma_2) - (\sigma_3 - \sigma_1)\right] \\
\epsilon_2 &= \frac{k_1}{3}\left[(\sigma_2 - \sigma_3) - (\sigma_1 - \sigma_2)\right] \\
\epsilon_3 &= \frac{k_1}{3}\left[(\sigma_3 - \sigma_1) - (\sigma_2 - \sigma_3)\right]
\end{aligned}\right\} \tag{A29}$$

Equation (A29) defines the plastic strains ϵ_1, ϵ_2, and ϵ_3 in terms of the principal stresses σ_1, σ_2, σ_3 and a plasticity modulus k_1.

For the case of simple tension $\sigma_2 = \sigma_3 = 0$, $\sigma_1 = \sigma$, and $\epsilon_1 = \epsilon$. Then by the first equation of equation (A29)

$$\epsilon = \frac{2k_1}{3}\sigma$$

or

$$k_1 = \frac{3}{2}\frac{\epsilon}{\sigma} \tag{A30}$$

Placing the value of k_1 from equation (A30) in equation (A29) gives

$$\left.\begin{aligned}
\frac{\epsilon_1}{\sigma_1 - \frac{1}{2}(\sigma_2 + \sigma_3)} &= \frac{\epsilon}{\sigma} \\
\frac{\epsilon_2}{\sigma_2 - \frac{1}{2}(\sigma_1 + \sigma_3)} &= \frac{\epsilon}{\sigma} \\
\frac{\epsilon_3}{\sigma_3 - \frac{1}{2}(\sigma_1 + \sigma_2)} &= \frac{\epsilon}{\sigma}
\end{aligned}\right\} \tag{A31}$$

Squaring both sides of equation (A31) and adding the numerators and denominators of the resulting equations yields

$$\frac{4\left(\epsilon_1^2 + \epsilon_2^2 + \epsilon_3^2\right)}{3\left[(\sigma_1 - \sigma_2)^2 + (\sigma_2 - \sigma_3)^2 + (\sigma_3 - \sigma_1)^2\right]} = \frac{\epsilon^2}{\sigma^2}$$

or

$$\frac{\epsilon}{\sigma} = \frac{\sqrt{\frac{2}{3}\left(\epsilon_1^2 + \epsilon_2^2 + \epsilon_3^2\right)}}{\sqrt{\frac{1}{2}\left[(\sigma_1 - \sigma_2)^2 + (\sigma_2 - \sigma_3)^2 + (\sigma_3 - \sigma_1)^2\right]}} \tag{A32}$$

Equation (A32) defines the relation between the principal plastic stresses and strains in terms of the stress and strain in simple tension. Equation (A32) may be written as

$$\frac{\epsilon}{\sigma} = \frac{\bar{\epsilon}}{\bar{\sigma}} \tag{A33}$$

where

$$\bar{\epsilon} = \sqrt{\frac{2}{3}\left(\epsilon_1^2 + \epsilon_2^2 + \epsilon_3^2\right)} = \frac{\sqrt{2}}{3}\sqrt{(\epsilon_1 - \epsilon_2)^2 + (\epsilon_2 - \epsilon_3)^2 + (\epsilon_3 - \epsilon_1)^2} \tag{A34}$$

and

$$\bar{\sigma} = \frac{1}{\sqrt{2}}\sqrt{(\sigma_1 - \sigma_2)^2 + (\sigma_2 - \sigma_3)^2 + (\sigma_3 - \sigma_1)^2} \tag{A35}$$

The strain $\bar{\epsilon}$ and stress $\bar{\sigma}$ as given by equations (A34) and (A35) will be called the significant stress and strain (references 7 to 11). Combined-stress test data may be represented in terms of $\bar{\sigma}$ and $\bar{\epsilon}$ as shown in figure 36 where $\bar{\sigma}$ and $\bar{\epsilon}$ are calculated by equations (A34) and (A35). Then by this theory and according to equation (A32) the

combined-stress curve in figure 36 should coincide with the stress-strain plot $\sigma - \epsilon$ for simple tension.

The stress $\bar{\sigma}$ and strain $\bar{\epsilon}$ have also been called the effective stress and strain by Dorn (reference 12). Furthermore, the significant stress and strain can be shown to be the same as the octahedral shear stress and strain as defined by Nadai (reference 14), when the octahedral shear stress and strain are replaced in terms of the normal stress and strain as given in equations (A33) to (A35).

A comparison of the significant stress value $\bar{\sigma}$ as given by equation (A35) with the expression for the distortion energy theory as given by equation (A23) shows that $\bar{\sigma}$ represents a uniaxial stress value with an elastic distortion energy value equal to the elastic distortion energy produced by the combined stresses σ_1, σ_2, and σ_3; that is, in plotting the significant stress-strain diagram the significant stress values give a plot of the square root of the elastic distortion energy multiplied by a constant. The identity between the significant stress and strain and the true stress-strain relation in tension assumed by this generalized St. Venant theory implies that the stress-strain relation in the plastic range under combined stresses is a function of the elastic distortion energy represented by these combined stresses.

Strain Equations for Combined Stresses

By assuming that the generalized St. Venant theory as defined by equations (A33) to (A35) applies, the $\bar{\sigma} - \bar{\epsilon}$ relation coincides with the $\sigma - \epsilon$ relation and equation (A11) may be written

$$\bar{\sigma} = k\bar{\epsilon}^n \tag{A36}$$

Then

$$\frac{\bar{\epsilon}}{\bar{\sigma}} = \frac{(\bar{\sigma})^{\frac{1-n}{n}}}{k^{1/n}} = \frac{1}{k^{1/n}} \left[\frac{(\sigma_1 - \sigma_2)^2 + (\sigma_2 - \sigma_3)^2 + (\sigma_3 - \sigma_1)^2}{2} \right]^{\frac{1-n}{2n}} \tag{A37}$$

Since $\frac{\bar{\epsilon}}{\bar{\sigma}} = \frac{\epsilon}{\sigma}$,

$$\frac{\epsilon}{\sigma} = \frac{1}{k^{1/n}} \left[\frac{(\sigma_1 - \sigma_2)^2 + (\sigma_2 - \sigma_3)^2 + (\sigma_3 - \sigma_1)^2}{2} \right]^{\frac{1-n}{2n}} \tag{A38}$$

On placing the value of ϵ/σ from equation (A38) in equation (A31), the principal plastic strains in terms of the stresses are

$$\left.\begin{aligned}
\epsilon_1 &= \left(\frac{\sigma_1}{k}\right)^{1/n} \left(\alpha^2 + \beta^2 - \alpha\beta - \alpha - \beta + 1\right)^{\frac{1-n}{2n}} \left(1 - \frac{\alpha}{2} - \frac{\beta}{2}\right) \\
\epsilon_2 &= \left(\frac{\sigma_1}{k}\right)^{1/n} \left(\alpha^2 + \beta^2 - \alpha\beta - \alpha - \beta + 1\right)^{\frac{1-n}{2n}} \left(\alpha - \frac{\beta}{2} - \frac{1}{2}\right) \\
\epsilon_3 &= \left(\frac{\sigma_1}{k}\right)^{1/n} \left(\alpha^2 + \beta^2 - \alpha\beta - \alpha - \beta + 1\right)^{\frac{1-n}{2n}} \left(\beta - \frac{\alpha}{2} - \frac{1}{2}\right)
\end{aligned}\right\} \quad \text{(A39)}$$

where α and β are the principal stress ratios

$$\left.\begin{aligned}
\alpha &= \sigma_2/\sigma_1 \\
\beta &= \sigma_3/\sigma_1
\end{aligned}\right\} \quad \text{(A40)}$$

where σ_1 is selected as the maximum principal stress so that α and β are less than 1.

Equation (A39) completely defines the plastic principal strains in terms of the principal stresses and the tension constants k and n. For biaxial stresses, $\sigma_3 = 0$ or $\beta = 0$, and equation (A39) becomes

$$\left.\begin{aligned}
\epsilon_1 &= \left(\frac{\sigma_1}{k}\right)^{1/n} \left(\alpha^2 - \alpha + 1\right)^{\frac{1-n}{2n}} \left(1 - \frac{\alpha}{2}\right) \\
\epsilon_2 &= \left(\frac{\sigma_1}{k}\right)^{1/n} \left(\alpha^2 - \alpha + 1\right)^{\frac{1-n}{2n}} \left(\alpha - \frac{1}{2}\right) \\
\epsilon_3 &= -\frac{1}{2}\left(\frac{\sigma_1}{k}\right)^{1/n} \left(\alpha^2 - \alpha + 1\right)^{\frac{1-n}{2n}} (\alpha + 1)
\end{aligned}\right\} \quad \text{(A41)}$$

Equations (A39) and (A41) give the plastic principal strains in terms of the principal stresses.

Fracture Strength Relations for Combined Stresses

There are not sufficient test data to confirm definitely a theory predicting stresses at fracture under combined stresses; however, test data for ductile materials subjected to biaxial tension and biaxial tension and compression are in closest agreement with the shear theory of failure. If σ_1 is the greatest principal stress and σ_3 is the algebraically smallest principal stress, then by the shear theory of rupture (references 5 and 6),

$$\frac{\sigma_1 - \sigma_3}{2} = \tau_r = \frac{\sigma_r}{2}$$

or

$$\sigma_1 - \sigma_3 = \sigma_r \tag{A42}$$

where σ_r is the rupture stress in simple tension.

For biaxial tensile stresses, $\sigma_3 = 0$ and equation (A42) becomes

$$\sigma_1 = \sigma_r \tag{A43}$$

For biaxial tensile and compressive stresses with $\sigma_1 > \sigma_2$, σ_1 in tension, σ_3 in compression, and $\sigma_2 = 0$, equation (A42) applies. Figure 37 is a graphical representation of the shear theory for biaxial stresses. For biaxial tensile stresses equation (A43) shows that the shear and stress theories are identical.

Ductility Relations for Combined Stresses

The ductility or maximum principal strain is determined by equation (A39) if the value for σ_1 at rupture is substituted. From equation (A42) this value of σ_1 is

$$\sigma_1 = \sigma_3 + \sigma_r$$

or

$$\sigma_1 = \sigma_r + \beta\sigma_1$$

or

$$\sigma_1 = \frac{\sigma_r}{(1 - \beta)} \tag{A44}$$

By using this value of σ_1 in equation (A39) the strains at rupture are

$$\left.\begin{aligned}
\epsilon_{1r} &= \left[\frac{\sigma_r}{k(1 - \beta)}\right]^{1/n}\left(\alpha^2 + \beta^2 - \alpha\beta - \alpha - \beta + 1\right)^{\frac{1-n}{2n}}\left(1 - \frac{\alpha}{2} - \frac{\beta}{2}\right) \\
\epsilon_{2r} &= \left[\frac{\sigma_r}{k(1 - \beta)}\right]^{1/n}\left(\alpha^2 + \beta^2 - \alpha\beta - \alpha - \beta + 1\right)^{\frac{1-n}{2n}}\left(\alpha - \frac{\beta}{2} - \frac{1}{2}\right) \\
\epsilon_{3r} &= \left[\frac{\sigma_r}{k(1 - \beta)}\right]^{1/n}\left(\alpha^2 + \beta^2 - \alpha\beta - \alpha - \beta + 1\right)^{\frac{1-n}{2n}}\left(\beta - \frac{\alpha}{2} - \frac{1}{2}\right)
\end{aligned}\right\} \tag{A45}$$

For biaxial stresses, $\sigma_3 = 0$, $\beta = 0$, and equation (A45) reduces to

$$\left.\begin{aligned}
\epsilon_{1r} &= \left(\frac{\sigma_r}{k}\right)^{1/n}\left(\alpha^2 - \alpha + 1\right)^{\frac{1-n}{2n}}\left(1 - \frac{\alpha}{2}\right) \\
\epsilon_{2r} &= \left(\frac{\sigma_r}{k}\right)^{1/n}\left(\alpha^2 - \alpha + 1\right)^{\frac{1-n}{2n}}\left(\alpha - \frac{1}{2}\right) \\
\epsilon_{3r} &= -\left(\frac{\sigma_r}{k}\right)^{1/n}\left(\alpha^2 - \alpha + 1\right)^{\frac{1-n}{2n}}\left(\frac{\alpha}{2} + \frac{1}{2}\right)
\end{aligned}\right\} \tag{A46}$$

Stress and Strain Values at Beginning of Necking for Combined Stresses

In order to determine the stresses and strains at beginning of necking, a procedure similar to that used for simple tension is applied. As for the case of simple tension, the beginning of necking is the point where the rate of strain hardening, which tends to increase the load resistance, is balanced by the decrease in load resistance caused by the decrease in the cross section. At this point a maximum load is reached which is followed by a decrease in load to rupture. The condition defining this point of instability is illustrated in the following paragraphs for the thin-walled cylinder subjected to internal pressure and axial load. For other members subjected to combined stresses a similar procedure can be used to determine the condition of instability.

Figure 38 shows a thin-walled cylinder subjected to an internal pressure p and an axial load P. If t and d are the initial wall thickness and internal diameter, respectively, and t_p and d_p represent the values of these dimensions in the plastic range, then for a thin-walled cylinder the longitudinal stress σ_1 and the circumferential stress σ_2 are

$$\sigma_1 = \frac{pd_p}{4t_p} + \frac{P}{\pi d_p t_p} \tag{A47}$$

and

$$\sigma_2 = \frac{pd_p}{2t_p} \tag{A48}$$

In order to determine the instability condition, it is necessary to distinguish two cases, one in which σ_2 is the greatest stress and the other in which σ_1 is the greatest stress.

Case 1 ($\sigma_2 > \sigma_1$).- For $\sigma_2 > \sigma_1$ a limiting pressure value p determines the instability and the stress σ_2 is used. Equation (A48) may be expressed in terms of the true strain ϵ_2 by noting that

$$t_p = t\, e^{-\epsilon_1 - \epsilon_2} \tag{A49}$$

and

$$d_p = d\, e^{\epsilon_2} \tag{A50}$$

where ϵ_1 and ϵ_2 are the true strains in the longitudinal and circumferential directions, respectively. (See appendix C.) Placing values of t_p and d_p from equations (A49) and (A50) in equation (A48) gives

$$p = 2\sigma_2 \left(\frac{t}{d}\right) e^{-\epsilon_2\left(2+\frac{\epsilon_1}{\epsilon_2}\right)} \tag{A51}$$

By equation (A41),

$$\frac{\epsilon_1}{\epsilon_2} = \frac{1 - \alpha/2}{\alpha - 1/2} = \frac{2 - \alpha}{2\alpha - 1} \tag{A52}$$

where

$$\alpha = \sigma_2/\sigma_1$$

Placing the value of ϵ_1/ϵ_2 as given by equation (A52) in equation (A49) gives

$$p = 2\sigma_2 \left(\frac{t}{d}\right) e^{-\epsilon_2\left(\frac{3\alpha}{2\alpha-1}\right)} \tag{A53}$$

The condition defining instability or beginning of necking is determined by the equation

$$dp = 0$$

or

$$dp = \frac{\partial p}{\partial \sigma_2} d\sigma_2 + \frac{\partial p}{\partial \epsilon_2} d\epsilon_2 = 0 \tag{A54}$$

Using the value of p from equation (A53) in equation (A54) gives

$$\frac{d\sigma_2}{d\epsilon_2} = \frac{3\alpha}{2\alpha - 1}\sigma_2 \tag{A55}$$

where

$$\alpha = \sigma_2/\sigma_1$$

Equation (A55) shows that necking or instability occurs where the slope of the true stress-strain curve for σ_2 equals $3\alpha/2\alpha - 1$ multiplied by the stress σ_2. Since by equation (A41) $\sigma_2 = f(\alpha)\epsilon_2^n$,

$$\frac{d\sigma_2}{d\epsilon_2} = nf(\alpha)\epsilon_2^{n-1}$$

By using the value of $\frac{d\sigma}{d\epsilon_2}$ from equation (A55)

$$\epsilon_2 = \frac{2\alpha - 1}{3\alpha} n \tag{A56}$$

that is, by equation (A55) instability occurs at a strain value ϵ_2 defined by equation (A56).

Case 2 $(\sigma_1 > \sigma_2)$.- For $\sigma_1 > \sigma_2$, a limiting axial load defines instability. The total axial force is

$$F = \pi d_p t_p \sigma_1 \tag{A57}$$

Placing values of t_p and d_p from equations (A49) and (A50) in equation (A48) gives

$$F = \pi dt\, e^{-\epsilon_1}\sigma_1 \tag{A58}$$

For instability,

$$dF = \frac{\partial F}{\partial \sigma_1} d\sigma_1 + \frac{\partial F}{\partial \epsilon_1} d\epsilon_1 = 0 \tag{A59}$$

From equations (A58) and (A59),

$$\frac{d\sigma_1}{d\epsilon_1} = \sigma_1 \tag{A60}$$

For instability in the axial direction the point of instability is defined when the slope of the true stress-strain curve $\sigma_1 - \epsilon_1$ equals the stress σ_1. Since by equation (A41) $\sigma_1 = f(\alpha)\epsilon_1^n$,

$$d\sigma_1/d\epsilon_1 = nf(\alpha)\epsilon_1^{n-1}$$

By using the value of $d\sigma_1/d\epsilon_1$ from equation (A60),

$$\epsilon_1 = n \tag{A61}$$

Equation (A61) determines the point of instability as the point on the $\bar{\epsilon} - \bar{\sigma}$ curve where ϵ_1 equals the constant n.

APPENDIX B

CORRECTION OF MEASURED ELASTIC STRAINS FOR LATERAL SENSITIVITY AND COMBINED-STRESS EFFECT

Baumberger (reference 3) shows that the correct strains, in terms of the measured strains based on the manufacturer's calibration, by using a simple tensile stress and steel, are

$$\left.\begin{aligned} e_{1e} &= \frac{(1 - \mu k_s)(\delta_1 - k_s\delta_2)}{(1 - k_s^2)} \approx (1 - \mu k_s)(\delta_1 - k_s\delta_2) \\ e_{2e} &= \frac{(1 - \mu k_s)(\delta_2 - k_s\delta_1)}{(1 - k_s^2)} \approx (1 - \mu k_s)(\delta_2 - k_s\delta_1) \end{aligned}\right\} \quad \text{(B1)}$$

where e_{1e} and e_{2e} are the corrected elastic strains in the longitudinal and lateral directions. The correction to the measured strains can be more conveniently determined than by using equation (B1); that is, the percent error in the measured strains can be found directly by solving equation (B1) for the measured strain δ_1; that is,

$$\delta_1 = \frac{e_{1e} + k_s e_{2e}}{(1 - k_s^2)(1 - \mu k_s)} \quad \text{(B2)}$$

The percent error in the strain e_{1e} is then

$$E_r = \frac{e_{1e} - \delta_1}{e_{1e}} 100 = \left[1 - \frac{e_{1e} + k_s e_{2e}}{(1 - k_s^2)(1 - \mu k_s)e_{1e}}\right] 100 \quad \text{(B3)}$$

But since $e_1 = \left(\sigma_{1e} - \mu\sigma_{2e}\right)/E$ and $e_2 = \left(\sigma_{2e} - \mu\sigma_{1e}\right)/E$, equation (B3) can be written

$$E_r = 100\left[1 - \frac{k_s - \mu + \left(\sigma_{1e}/\sigma_{2e}\right)\left(1 - k_s\mu\right)}{\left(1 - k_s^2\right)\left(1 - \mu k_s\right)\left(\frac{\sigma_{1e}}{\sigma_{2e}} - \mu\right)}\right] \tag{B4}$$

Since $k_s = 0.021$ for the SR-4 gages used, $\left(1 - k_s^2\right)$ is approximately equal to 1, and equation (B4) becomes

$$E_r = 100\left[\frac{\left(\mu^2 - 1\right) k_s}{\left(1 - \mu k_s\right)\left(\frac{\sigma_{1e}}{\sigma_{2e}} - \mu\right)}\right] \tag{B5}$$

For the aluminum alloy tested, $\mu = 0.33$, so that equation (B5) reduces to

$$E_r = \frac{-1.9\alpha}{1 - 0.33\alpha} \tag{B6}$$

where α equals the principal stress ratio σ_{2e}/σ_{1e}. For a given principal stress ratio α, equation (B6) determines the percent correction to be applied to the measured elastic strains.

APPENDIX C

EQUATIONS FOR WALL THICKNESS AND DIAMETER OF TUBULAR SPECIMEN IN THE PLASTIC RANGE

In the plastic range of stresses the original values of the wall thickness t and internal diameter d can no longer be used to calculate the stresses, and the actual values of the wall thickness t_p and internal diameter d_p must be used.

The true unit strain in the direction of the wall thickness t_p is, by using the definition of true strain (appendix A),

$$\epsilon_3 = \log_e \frac{t_p}{t} \tag{C1}$$

Since the volume is assumed to be constant in the plastic range,

$$\left.\begin{aligned} &\epsilon_1 + \epsilon_2 + \epsilon_3 = 0 \\ \text{or} \quad &\epsilon_3 = -\left(\epsilon_1 + \epsilon_2\right) \end{aligned}\right\} \tag{C2}$$

From equations (C1) and (C2),

$$t_p = t \log_e^{-1}\left(-\epsilon_1 - \epsilon_2\right) \tag{C3}$$

The relations between the true strains ϵ_1 and ϵ_2 in the lateral and longitudinal directions in terms of the nominal strains e_1 and e_2 in these directions are (appendix A)

$$\epsilon_1 = \log_e (1 + e_1) \tag{C4}$$

$$\epsilon_2 = \log_e (1 + e_2) \tag{C5}$$

By adding equations (C4) and (C5) and taking the antilogarithm of the resulting equation,

$$\log_e{}^{-1}\left(-\epsilon_1 - \epsilon_2\right) = \frac{1}{\left(1 + e_1\right)\left(1 + e_2\right)} \tag{C6}$$

From equations (C3) and (C6),

$$t_p = \frac{t}{\left(1 + e_1\right)\left(1 + e_2\right)} = \frac{t}{1 + e_1 + e_2 + e_1 e_2} \tag{C7}$$

Since $e_1 e_2$ is small compared with e_1 and e_2, equation (C7) may be written

$$t_p = \frac{t}{1 + e_1 + e_2} \tag{C8}$$

The internal diameter d_p in the plastic range equals the external diameter minus twice the wall thickness, or

$$d_p = d_p' - 2t_p \tag{C9}$$

The external diameter d_p' in terms of the nominal lateral strain e_2 is equal to

$$d_p' = (d + 2t)(1 + e_2) \tag{C10}$$

From equations (C9) and (C10) the internal diameter becomes

$$d_p = (d + 2t)(1 + e_2) - 2t_p \qquad (C11)$$

where t_p is determined by equation (C8).

REFERENCES

1. Hollomon, J. H.: Tensile Deformation. Tech. Pub. No. 1879, Metals Technology, June 1945.

2. Low, John R., Jr., and Prater, T. A.: Plastic Flow of Aluminum Aircraft Sheet under Combined Loads. II - (NA-150). OSRD No. 4052, Serial No. M-328, War Metallurgy Div., NDRC, Aug. 22, 1944.

3. Timoshenko, S.: Strength of Materials. Part II - Advanced Theory and Problems. Second ed., D. Van. Nostrand Co., Inc., 1941.

4. Baumberger, R., and Hines, F.: Practical Reduction Formulas for Use on Bonded Wire Strain Gages in Two-Dimensional Stress Fields. Proc. Soc. Exp. Stress Analysis, vol. II, no. 1, 1944, pp. 113–127.

5. Marin, J.: Mechanical Properties of Materials and Design. McGraw-Hill Book Co., Inc., 1942.

6. Marin, J.: A New Method of Defining Failure in Members Subjected to Combined Stresses. Trans. Am. Soc. Metals, vol. 29, no. 4, 1941, p. 1013.

7. Gensamer, M., Lankford, W. T., Jr., Ransom, J. T., and Vajda, John: Plastic Flow of Aluminum Aircraft Sheet under Combined Loads (NA-149) (NA-150). I - Development of Tests for Forming Limits; Stress-Strain Curves under Combined Loads. OSRD No. 5282, Serial No. M-527, War Metallurgy Div., NDRC, June 29, 1945.

8. Gensamer, M., Lankford, W. T., Jr., Prater, T. A., Vajda, John, and Ransom, J. T.: Plastic Flow of Aluminum Aircraft Sheet under Combined Loads (NA-149) (NA-150). II - Forming Limits for Aircraft Sheets at Room Temperature. OSRD No. 5283, Serial No. M-528, War Metallurgy Div., NDRC, June 29, 1945.

9. Gensamer, M., Lankford, W. T., Jr., and Vajda, John: Plastic Flow of Aluminum Aircraft Sheet under Combined Loads (NA-149) (NA-150). III - Effect of Aging at Room Temperature on the Properties of 75S in the Circular Hydraulic Bulge Test. OSRD No. 4832, Serial No. M-468, War Metallurgy Div., NDRC, Dec. 15, 1944.

10. Gensamer, M., Lankford, W. T., Jr., Saibel, E. A., Prater, T. A., Ransom, J. T., and Vajda, John: Plastic Flow of Aluminum Aircraft Sheet under Combined Loads (NA-149) (NA-150). IV - Theory of Forming Limits. OSRD No. 5284, Serial No. M-529, War Metallurgy Div., NDRC, June 29, 1945.

11. Saibel, E. A., Ransom, J. T., Lankford, W. T., Jr., and Gensamer, M.: Plastic Flow of Aluminum Aircraft Sheet under Combined Loads (NA-149) (NA-150). V - Strain Distribution in Formed Parts. OSRD No. 5264, Serial No. M-530, War Metallurgy Div., NDRC, June 29, 1945.

12. Dorn, J. E., and Thomsen, E. G.: The Effect of Combined Stresses on the Ductility of Metals. OSRD No. 3218, Serial No. M-213, War Metallurgy Div., NDRC, Feb. 2, 1944.

13. Jelinek, J. J., Latter, A. J., and Thomsen, E. G.: Plastic Flow in Metals. OPRD Rep. No. W-200, May 1945.

14. Nadai, A., and Davis, E. A.: Plastic Behavior of Metals in the Strain-Hardening Range. Parts I and II. Jour. Appl. Phys., vol. 8, no. 3, March 1937, pp. 205-217.

15. Bridgman, P. W.: The Stress Distribution at the Neck of a Tensile Specimen. Trans. Am. Soc. Metals, vol. 32, 1944, p. 553.

16. Gensamer, M.: Strength and Ductility. Trans. Am. Soc. Metals, vol. 36, no. 1, 1946, pp. 30-60.

TABLE 1.- MECHANICAL PROPERTIES OF 24S-T ALUMINUM ALLOY BASED ON TENSION CONTROL TESTS

[Designations B, C, and D in first column refer to specimens cut from tubes B, C, and D]

Specimen	Nominal stress-strain results				True stress-strain results			
	Yield stress (0.2-percent offset) (psi)	Ultimate stress (psi)	Modulus of elasticity (psi)	Elongation in 2 in. (percent)	Fracture stress (psi)	True ductility (in./in.)	Constant, k (psi)	Constant, n
T1B	----------	71.2×10^3	----------	9.4	80.0×10^3	11.8×10^2	----------	----
T2B	----------	72.4	----------	8.6	79.0	9.0	----------	----
T3B	----------	72.9	----------	7.8	79.4	8.6	----------	----
T4B	----------	72.0	----------	8.6	78.6	8.9	----------	----
Average	48.5×10^3	72.1	10.6×10^6	8.6	79.3	9.6	1.20×10^5	0.18
T1C	----------	75.0	----------	10.2	83.5	10.8	----------	----
T2C	----------	74.0	----------	8.6	80.5	8.5	----------	----
T3C	----------	71.4	----------	7.8	77.4	8.1	----------	----
T4C	----------	69.8	----------	6.3	76.5	9.2	----------	----
Average	50.0	72.6	10.8	8.2	79.5	9.2	1.15	0.16
T1D	----------	72.0	----------	8.6	78.5	8.9	----------	----
T2D	----------	72.8	----------	8.6	80.2	9.5	----------	----
T3D	----------	72.4	----------	7.8	78.4	7.9	----------	----
T4D	----------	67.6	----------	6.3	72.0	6.4	----------	----
Average	50.0	71.2	10.8	7.8	77.3	8.2	1.08	0.15
Over-all average	49.5	72.0	10.7	8.2	78.7	9.0	1.14	0.16

TABLE 2.- YIELD STRESSES FOR VARIOUS RATIOS OF BIAXIAL STRESSES

Biaxial stress ratio, $\alpha = \frac{\sigma_2}{\sigma_1}$	Yield stress, σ_{1y} (psi)	Yield stress, σ_{2y} (psi)	Yield stress, σ_{3y} (psi)	Stress ratios	
				$x = \frac{\sigma_{1y}}{\sigma_y}$	$y = \frac{\sigma_{2y}}{\sigma_y}$
0 (longitudinal tension)	47.5×10^3	0	0	1.00	0
.25	49.8	13.0×10^3	-1.3×10^3	1.05	.27
.50	54.7	26.6	-2.9	1.15	.56
.75	53.9	41.4	-4.2	1.13	.87
1.00	49.7	51.1	-5.1	1.04	1.07
1.33	39.7	53.8	-5.4	.84	1.13
2.00	23.6	47.3	-4.9	.50	1.00
∞ (transverse tension)	0	43.2	-4.3	0	.91

TABLE 3.- NOMINAL ULTIMATE STRESSES FOR VARIOUS BIAXIAL STRESS RATIOS

Biaxial stress ratio, $\alpha = \frac{\sigma_2}{\sigma_1}$	Specimen	Nominal ultimate stress, σ_{1u} (psi)	Nominal ultimate stress, σ_{2u} (psi)	Stress ratio, $x = \frac{\sigma_{1u}}{\sigma_u}$	Stress ratio, $y = \frac{\sigma_{2u}}{\sigma_u}$
0 (longitudinal tension)	B8	78.3×10^3	0	1.00	0
	B10	81.0	0	1.03	0
	C10	78.0	0	1.00	0
	D8	75.9	0	.97	0
	D10	77.9	0	1.00	0
	Average	$\sigma_u = 78.2$	0	1.00	0
.25	[a]B5	68.8	17.9×10^3	.88	.23
	C4	84.6	23.6	.98	.30
	D4	76.6	20.0	.98	.26
	Average	80.6	21.8	.98	.28
.5	B3	79.4	42.0	1.01	.54
	C5	80.5	42.0	1.03	.54
	[a]D5	71.8	37.5	.92	.48
	Average	80.0	42.0	1.02	.54
.75	B7	78.0	61.5	1.00	.79
	C6	82.9	64.0	1.06	.82
	C7	80.0	62.5	1.02	.80
	D6	83.0	64.6	1.06	.83
	Average	81.0	63.2	1.04	.81
1.00	B4	61.5	64.0	.79	.82
	C1	62.0	64.5	.79	.82
	D1	56.5	59.0	.72	.75
	Average	60.0	62.5	.77	.80
1.33	B2	45.2	63.0	.58	.81
	C3	40.4	56.4	.52	.72
	C8	46.0	64.0	.59	.82
	D3	46.0	64.1	.59	.82
	Average	44.4	61.9	.57	.79
2.0	B6	29.4	61.5	.38	.79
	C2	29.6	62.0	.38	.79
	D2	30.8	61.5	.39	.79
	Average	29.9	61.7	.38	.79
∞ (transverse tension)	B9	0	63.5	0	.81
	C9	0	62.5	0	.80
	D9	0	61.5	0	.79
	Average	0	62.5	0	.80

[a]Values not included in determining averages.

TABLE 4.- TRUE FRACTURE STRESSES FOR VARIOUS BIAXIAL STRESS RATIOS

Biaxial stress ratio, $\alpha = \frac{\sigma_2}{\sigma_1}$	Specimen	True fracture stresses, σ_{1r} (psi)	True fracture stresses, σ_{2r} (psi)	Stress ratio, $x = \frac{\sigma_{1r}}{\sigma_r}$	Stress ratio, $y = \frac{\sigma_{2r}}{\sigma_r}$
0 (longitudinal tension)	B8	92.6×10^3	0	1.02	0
	B10	92.5	0	1.02	0
	C10	89.0	0	.99	0
	D8	88.0	0	.98	0
	D10	91.2	0	1.00	0
	Average	$\sigma_r = 90.7$	0	1.00	0
.25	[a]B5	74.9	18.9×10^3	.83	.21
	C4	89.4	24.1	.99	.27
	D4	81.8	20.7	.90	.23
	Average	85.6	22.4	.95	.25
.50	B3	87.6	46.1	.96	.51
	C5	88.8	45.7	.98	.50
	[a]D5	75.0	39.2	.83	.43
	Average	88.2	45.9	.97	.51
.75	B7	91.1	75.2	1.00	.83
	C6	94.8	75.2	1.04	.83
	C7	92.4	74.4	1.01	.82
	D6	95.2	76.8	1.05	.84
	Average	93.4	75.4	1.03	.83
1.0	B4	71.8	79.0	.79	.87
	C1	71.6	77.3	.79	.85
	D1	62.3	66.8	.69	.74
	Average	68.6	74.4	.76	.82
1.33	B2	51.0	71.5	.56	.79
	C3	47.0	67.6	.52	.75
	C8	54.1	77.8	.60	.85
	D3	53.1	75.2	.59	.83
	Average	51.3	73.0	.57	.81
2	B6	33.3	66.6	.37	.73
	C2	36.8	73.6	.41	.81
	D2	36.8	73.7	.41	.81
	Average	35.6	71.3	.39	.78
∞ (transverse tension)	B9	0	77.2	0	.85
	C9	0	72.3	0	.80
	D9	0	76.2	0	.84
	Average	0	75.2	0	.83

[a]Values not included in determining averages.

TABLE 5.- NOMINAL AND TRUE DUCTILITY VALUES FOR VARIOUS BIAXIAL STRESS RATIOS

Biaxial stress ratio	Specimen	Nominal ductility (in./in.)	True ductility (in./in.)
0 (longitudinal tension)	B8	15.6×10^{-2}	14.5×10^{-2}
	B10	13.9	13.0
	C10	15.2	14.1
	D8	14.1	13.1
	D10	14.1	13.1
	Average	14.6	13.6
.25	B5	9.3	8.9
	C4	6.3	6.1
	D4	7.8	7.5
	Average	7.8	7.5
.50	B3	10.8	10.2
	C5	7.8	7.5
	D5	4.0	4.5
	Average	7.5	7.4
.75	B7	12.5	11.8
	C6	9.5	9.1
	C7	10.9	10.3
	D6	9.2	8.8
	Average	10.5	10.0
1.0	B4	7.8	7.5
	C1	6.4	6.2
	D1	4.5	4.4
	Average	6.2	6.0
1.33	B2	4.9	4.8
	C3	12.5	11.8
	C8	13.9	13.0
	D3	6.8	6.6
	Average	9.5	9.1
2.0	B6	6.4	6.2
	C2	8.6	8.2
	D2	8.6	8.2
	Average	7.9	7.5
∞ (transverse tension)	B9	10.0	9.5
	C9	7.8	7.5
	D9	10.7	10.2
	Average	9.5	9.1

TABLE 6.- TRUE STRESS-STRAIN CONSTANTS FOR UNIAXIAL TENSION TESTS

Direction of stress	Specimen	Nominal ultimate stress (psi)	True fracture stress (psi)	True ductility (in./in.)	Constant, k (psi)	Constant, n
Longitudinal (tubes)	B8	78.3	92.6	14.5	----------	----------
	B10	81.0	92.5	13.0	----------	----------
	C10	78.0	89.0	14.1	----------	----------
	D8	75.9	88.0	13.1	----------	----------
	D10	77.9	91.2	13.1	----------	----------
	Average	78.2	90.7	13.6	1.14×10^5	0.22
Transverse (tubes)	B9	63.5	77.2	9.5	----------	----------
	C9	62.5	72.3	7.5	----------	----------
	D9	61.5	76.2	10.2	----------	----------
	Average	62.7	75.2	9.1	1.15	.19
Longitudinal (control test)	Specimen from tube B	72.1	79.3	9.6	1.20	.18
	Specimen from tube C	72.6	79.5	9.3	1.15	.16
	Specimen from tube D	71.2	77.3	8.2	1.08	.15
	Average	72.0	78.7	9.0	1.14	.16

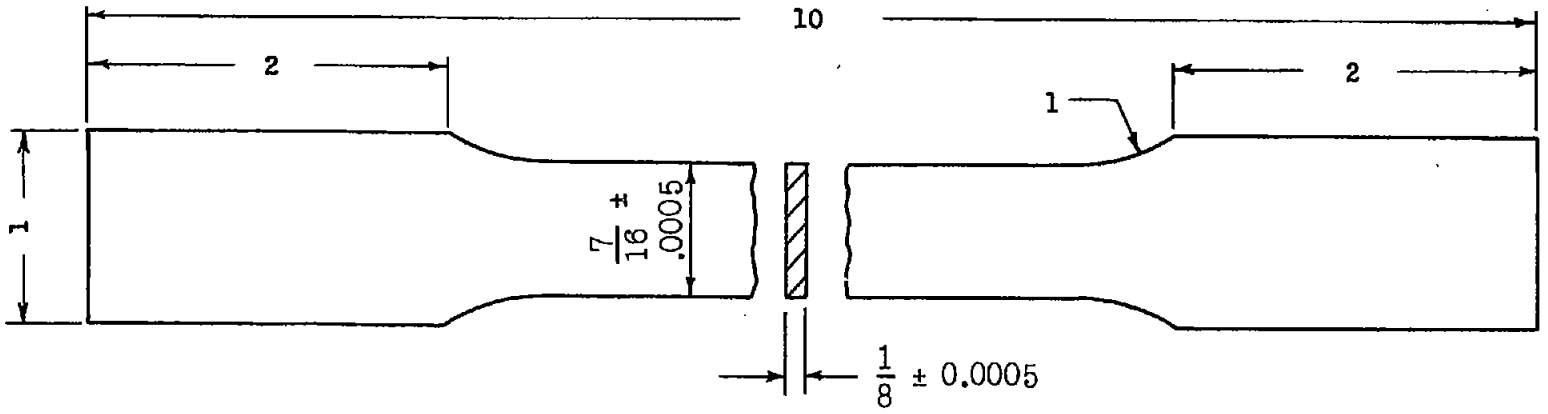

Figure 1.- Tensile control specimen. All dimensions are in inches.

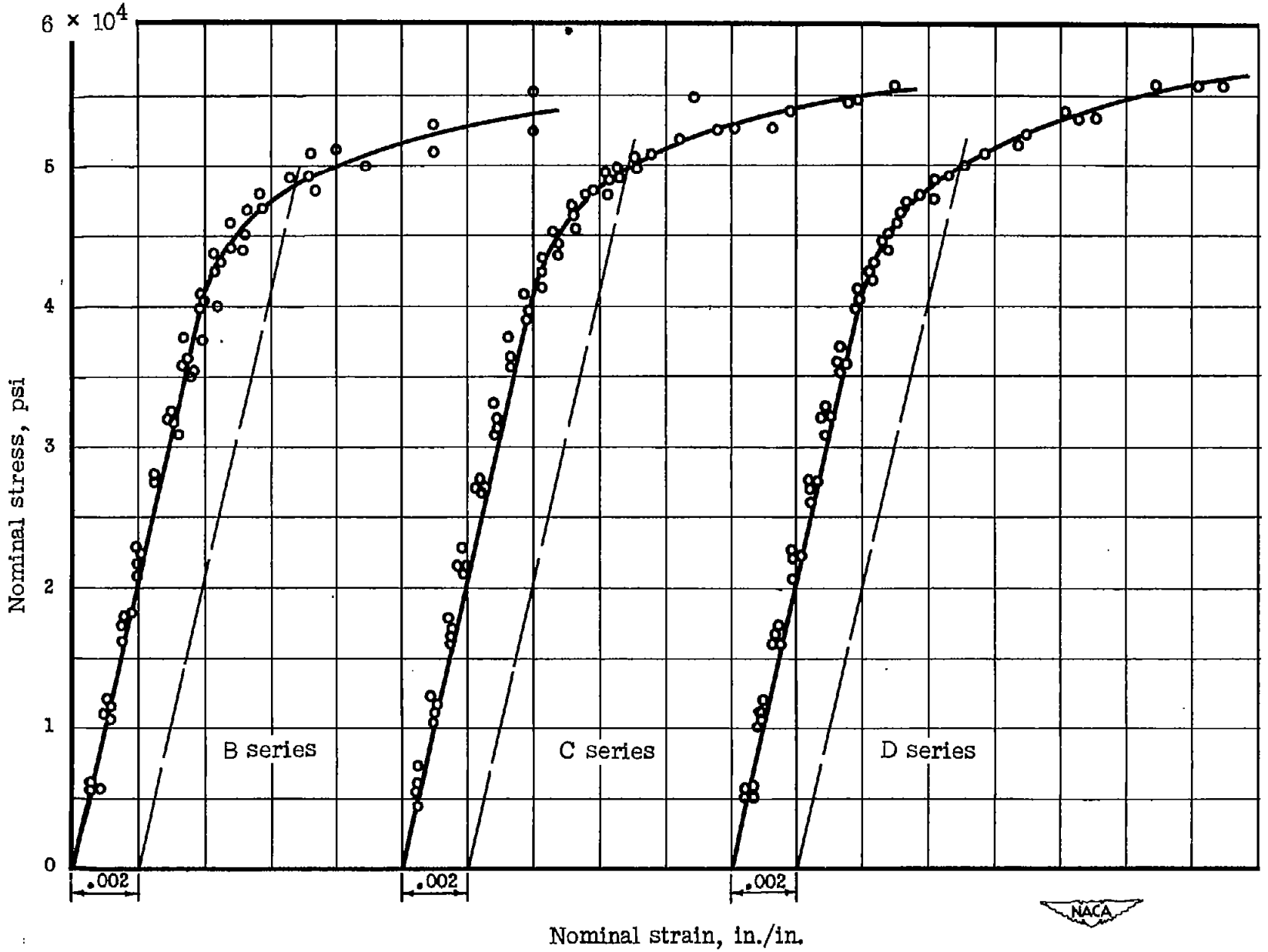

Figure 2.- Conventional stress-strain diagrams for tension control specimens.

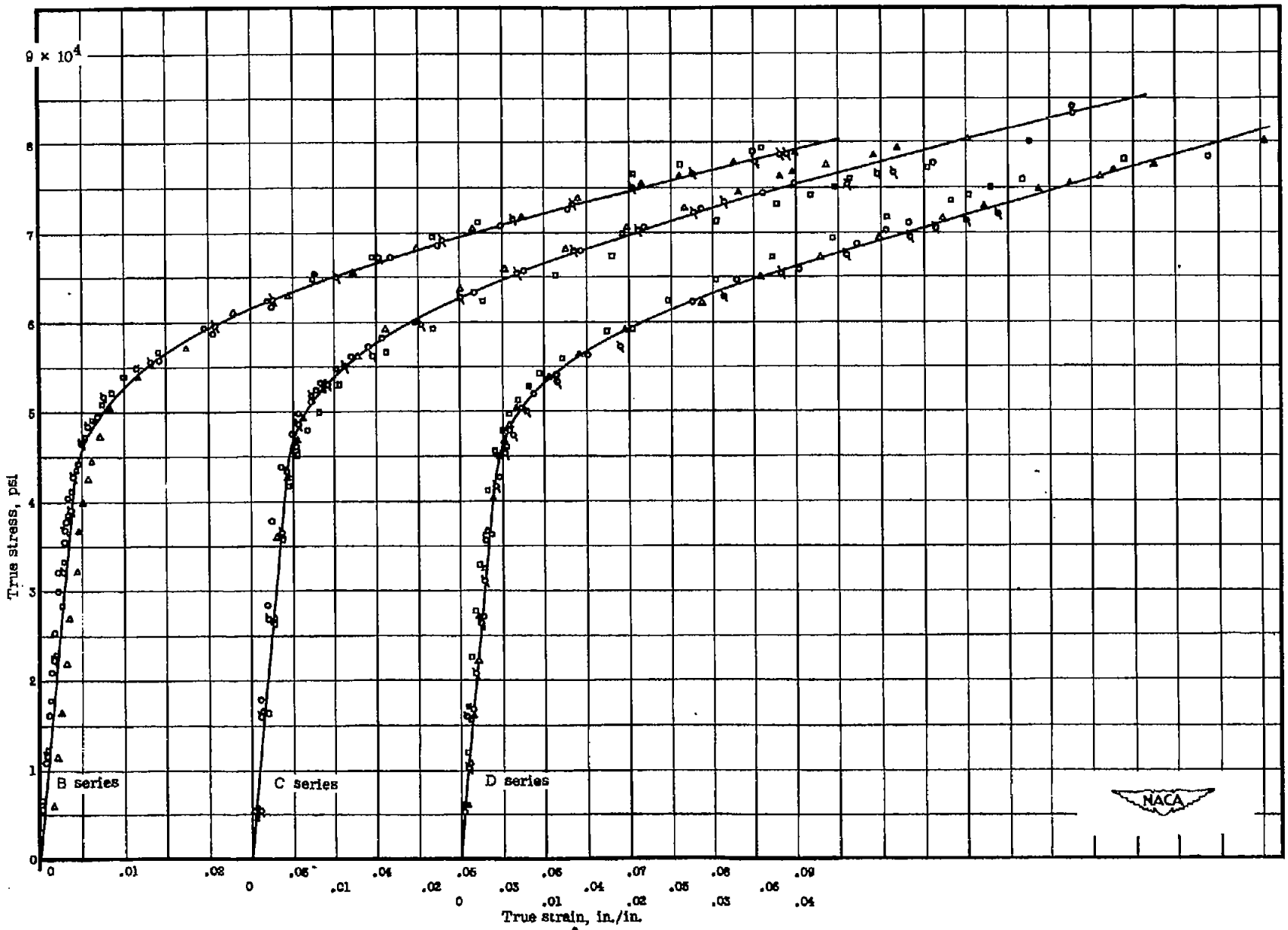

Figure 3.- True stress-strain diagrams for tension control specimens.

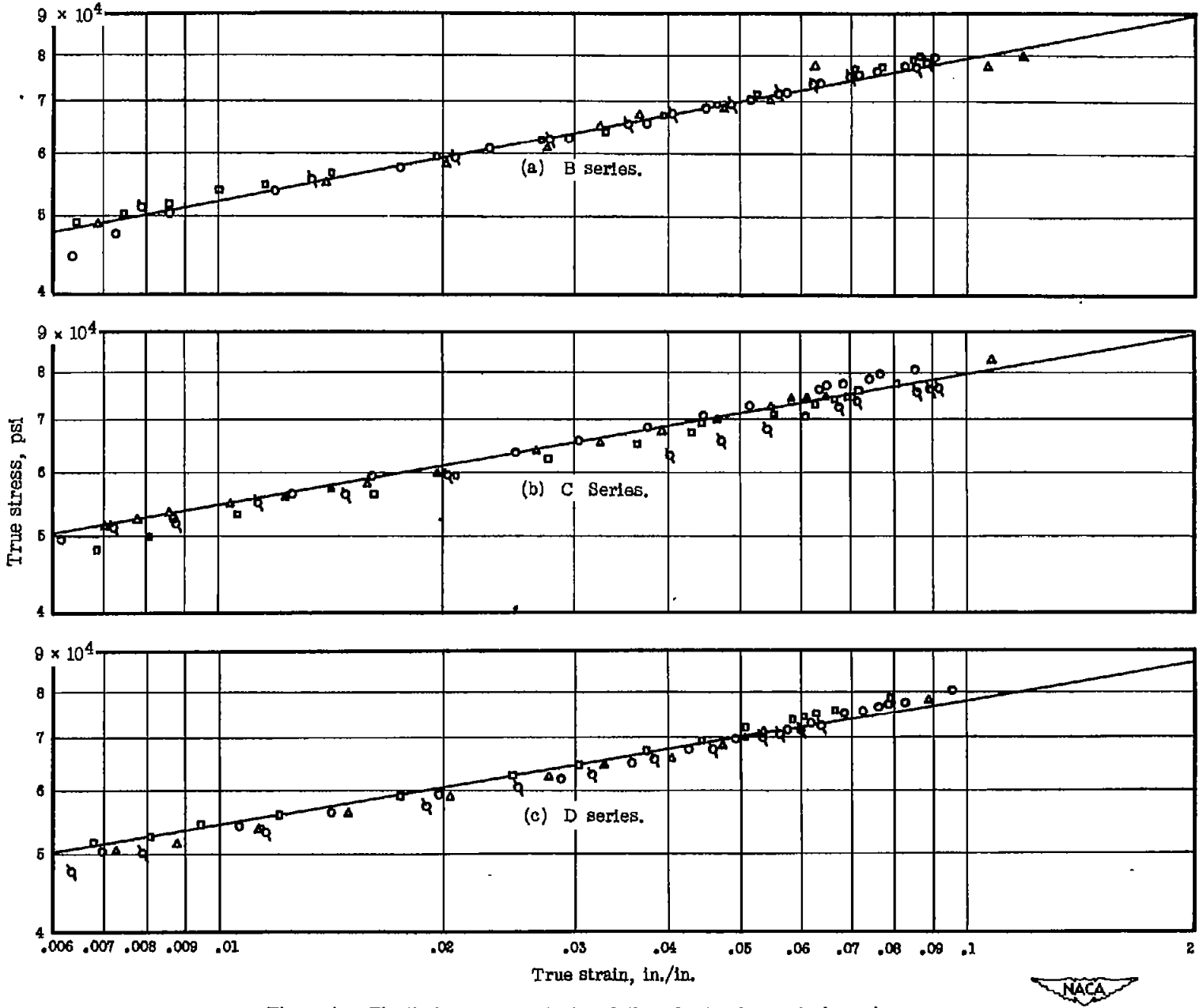

Figure 4.- Plastic true stress-strain relations for tension control specimens.

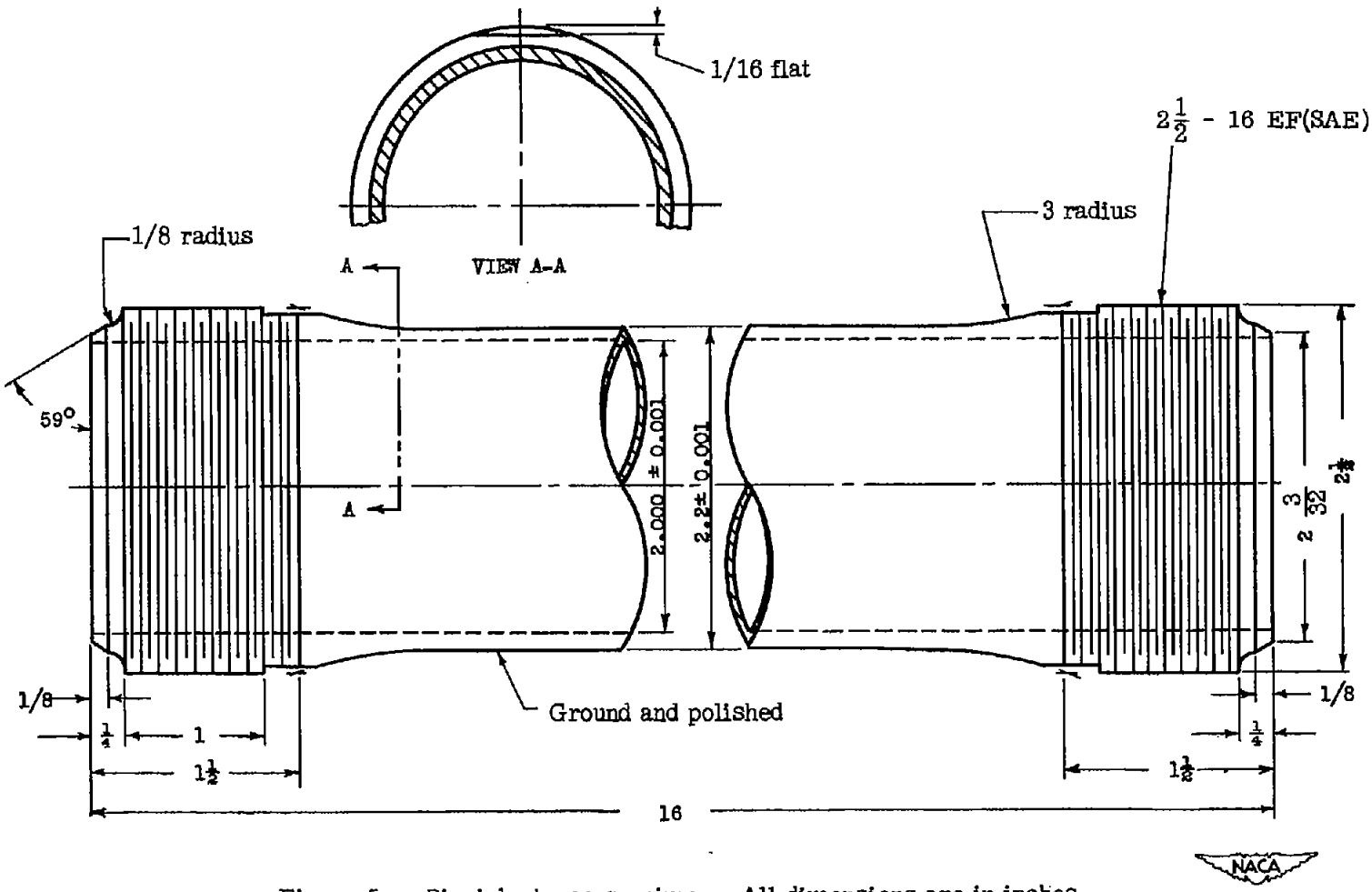

Figure 5.- Biaxial-stress specimen. All dimensions are in inches.

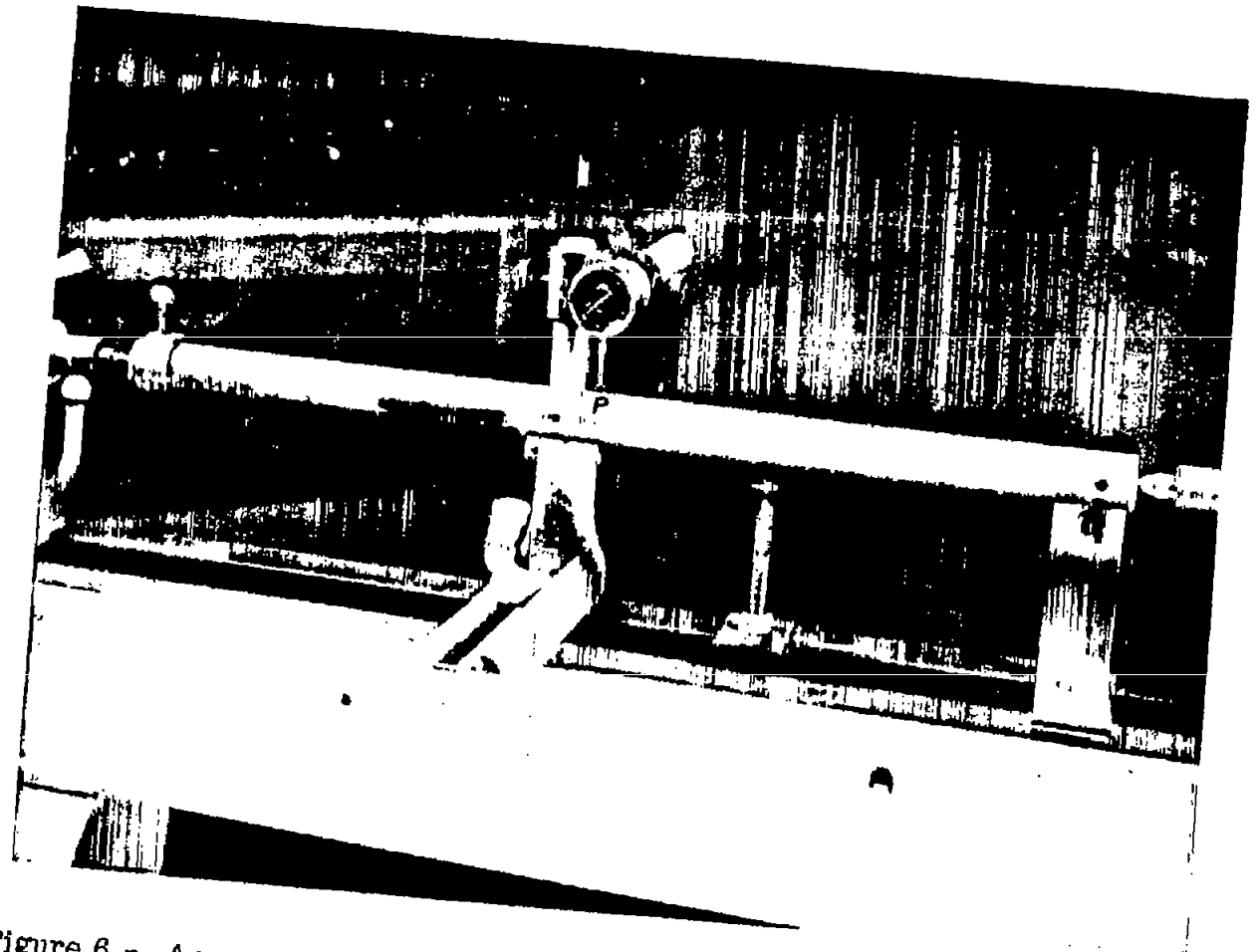

Figure 6.- Apparatus for measuring wall thickness of biaxial-stress specimens.

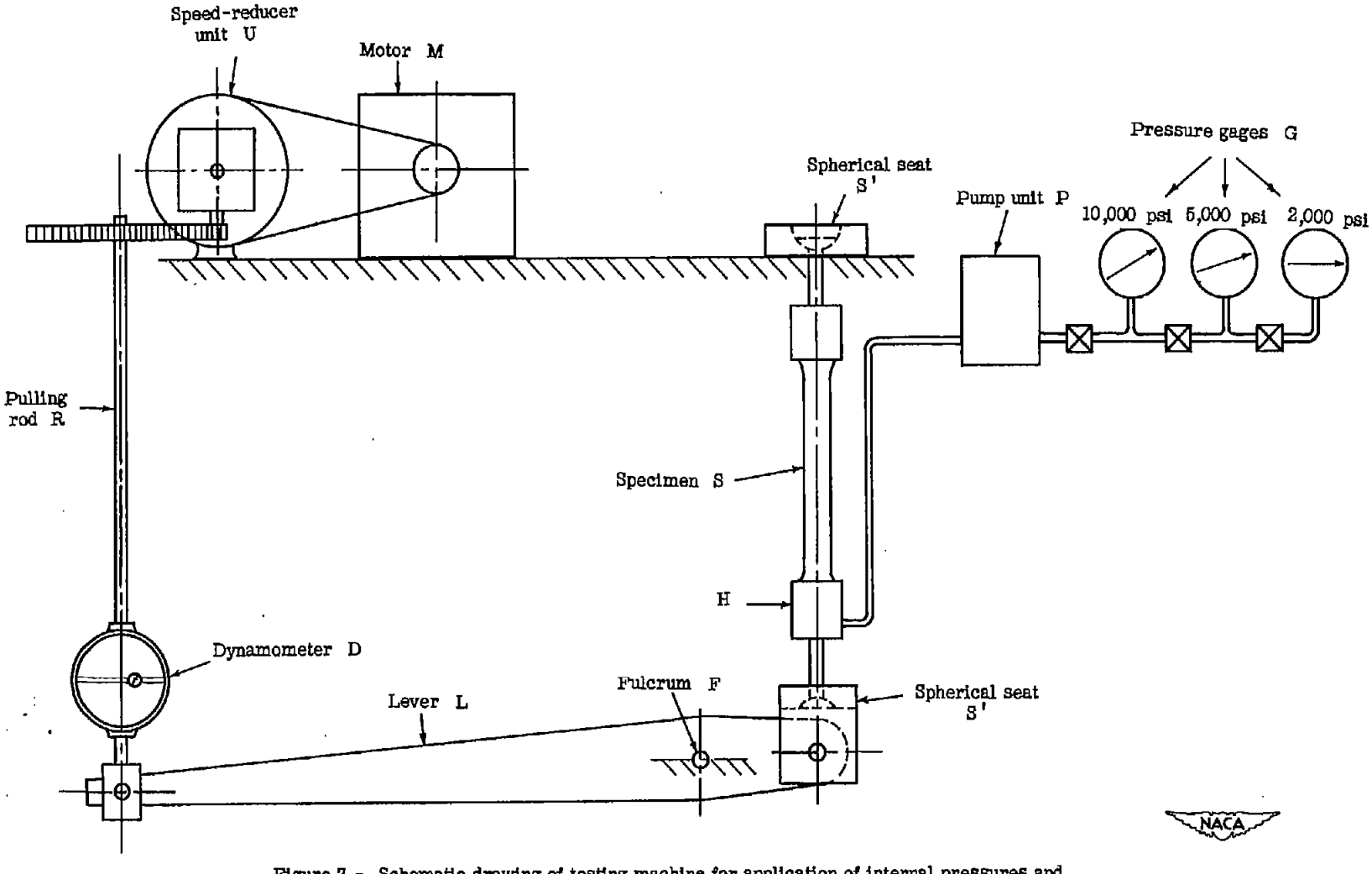

Figure 7.- Schematic drawing of testing machine for application of internal pressures and axial loads to a tubular specimen.

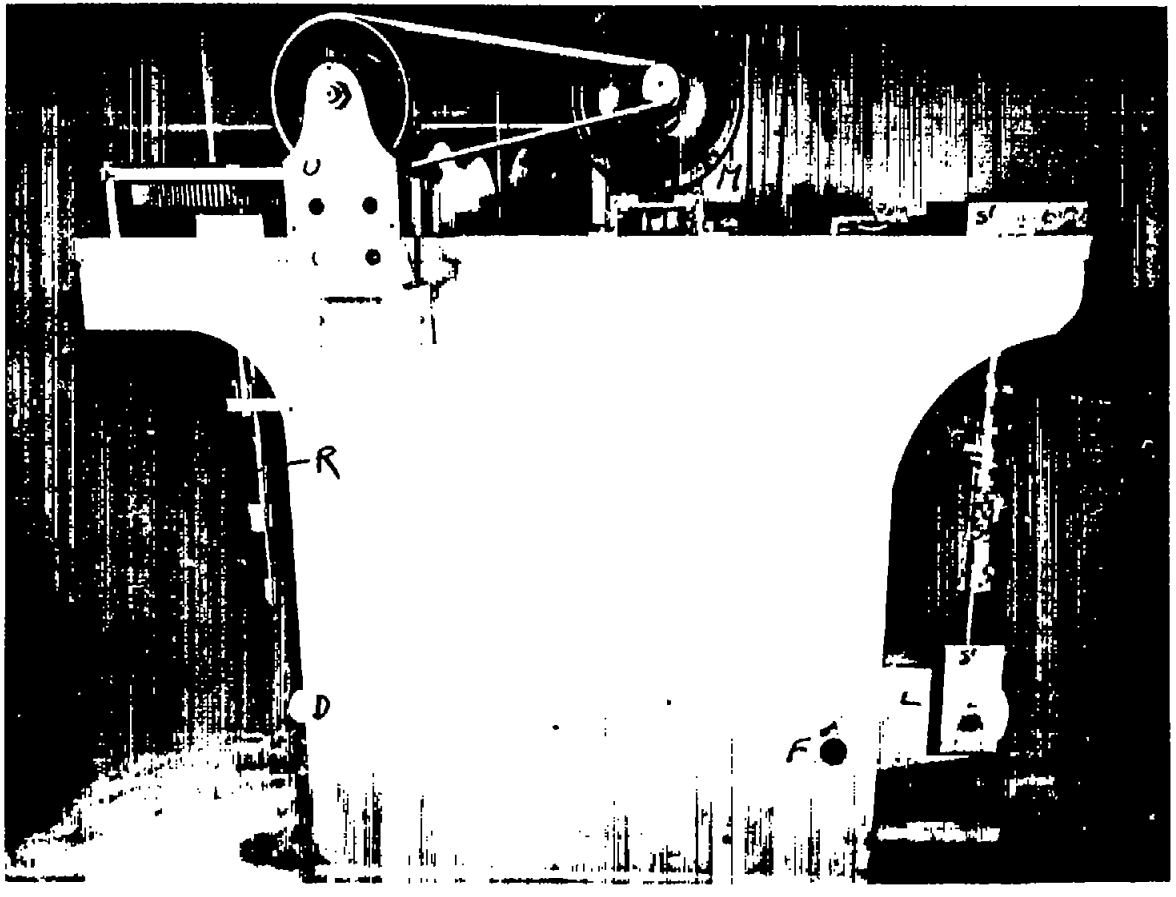

Figure 8.- Biaxial testing machine showing method of applying axial load.

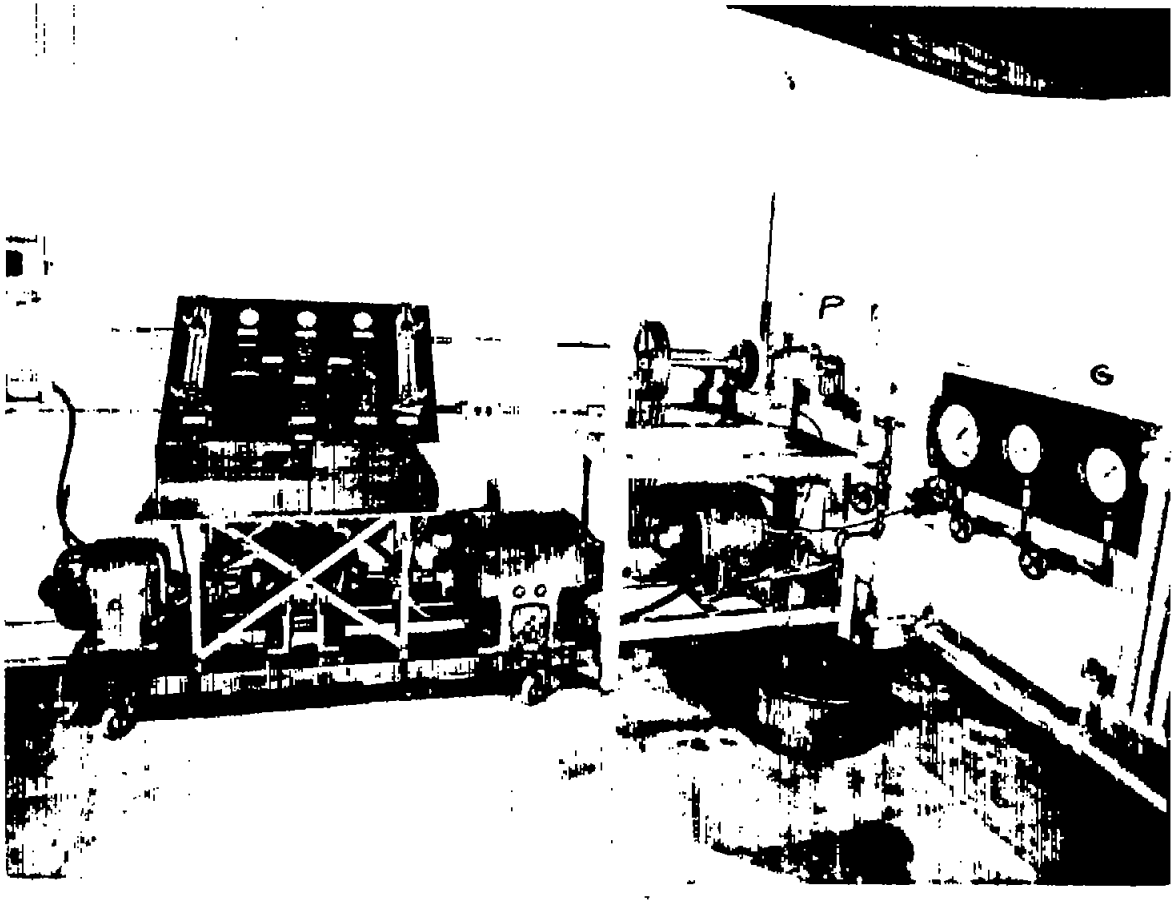

Figure 9.- Apparatus for application of internal pressure to tubular specimen.

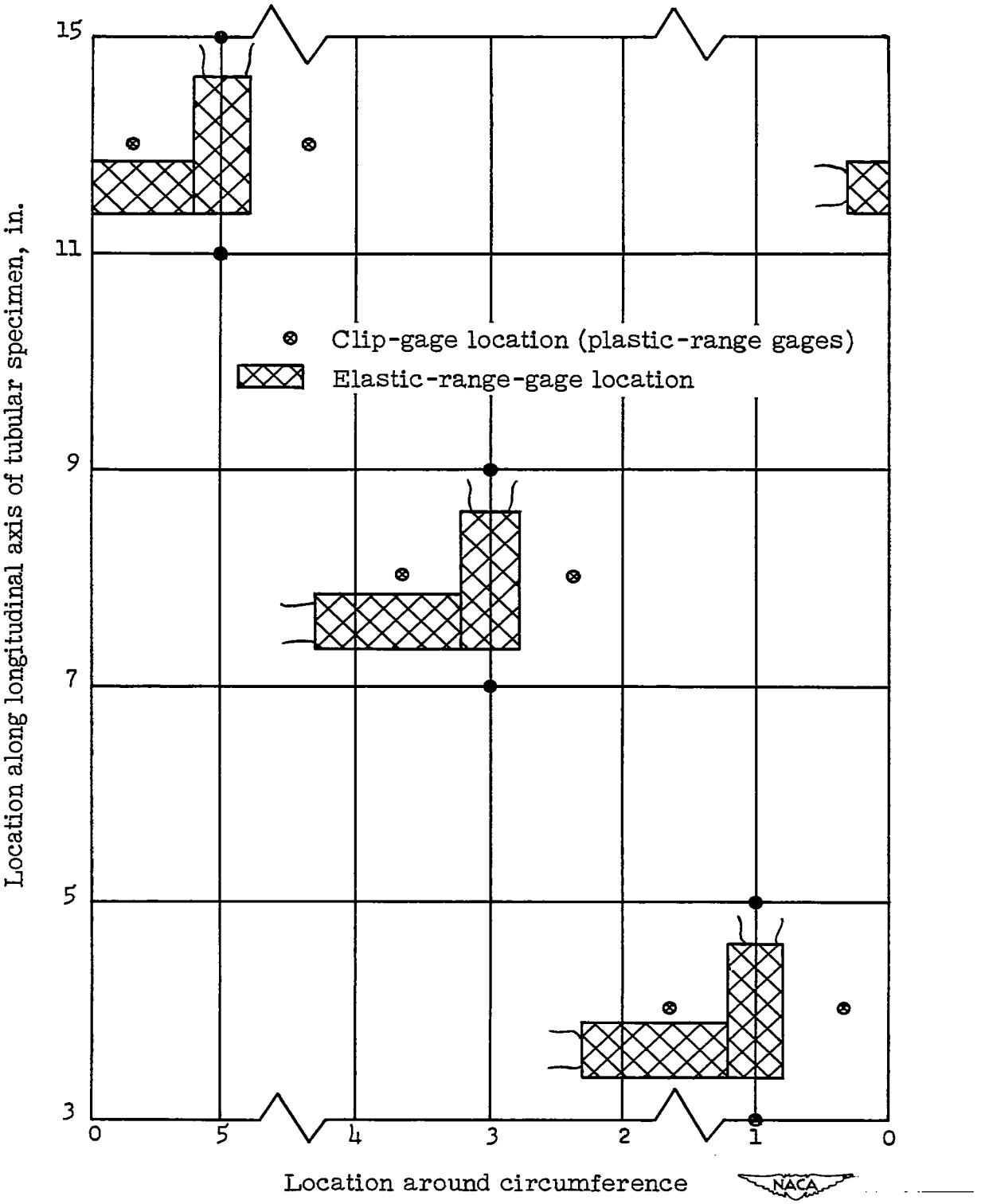

Figure 10.- Developed surface of tubular specimen showing location of elastic-range and plastic-range gages.

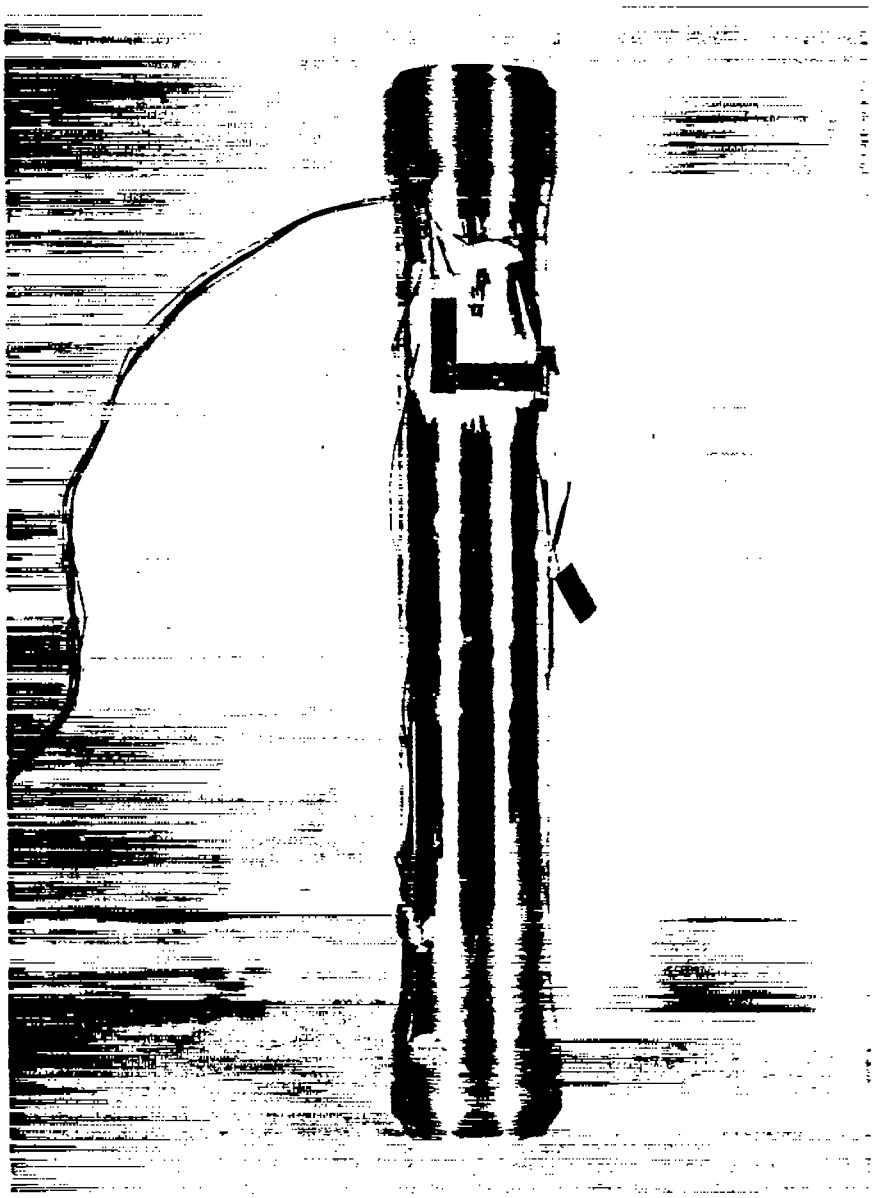

Figure 11.- Tubular specimen showing SR-4 electric strain gages for measuring elastic strains.

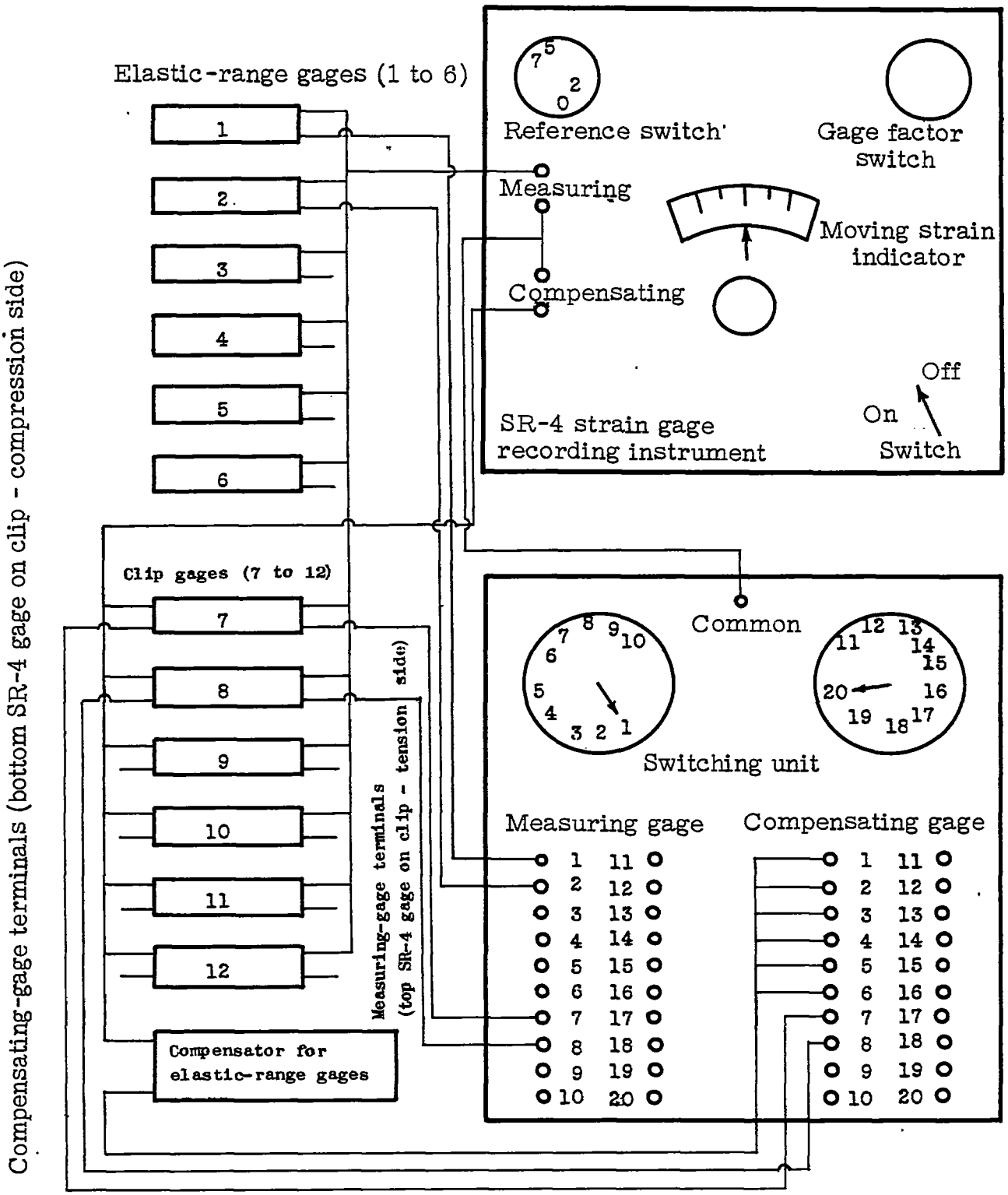

Figure 12.- Wiring diagram for strain measurements.

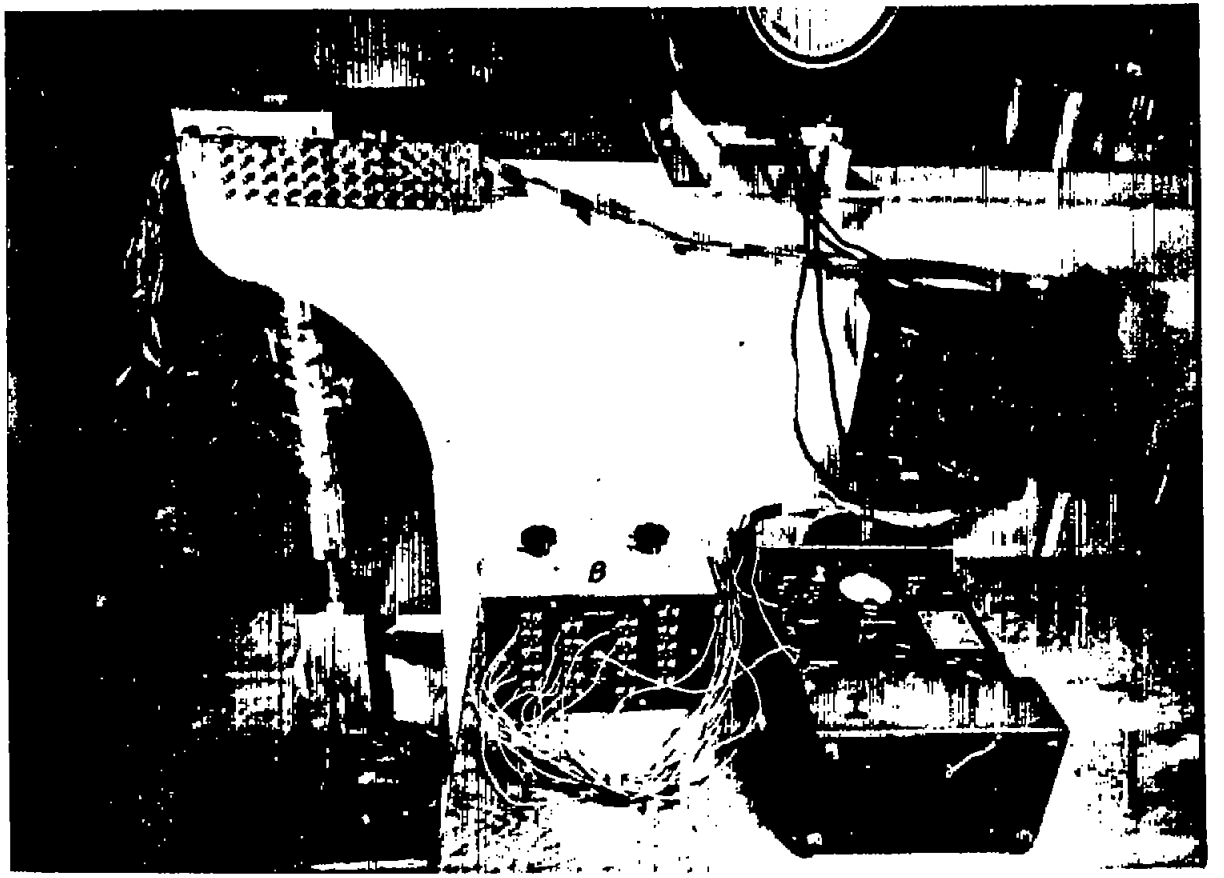

Figure 13.- Strain-measuring apparatus.

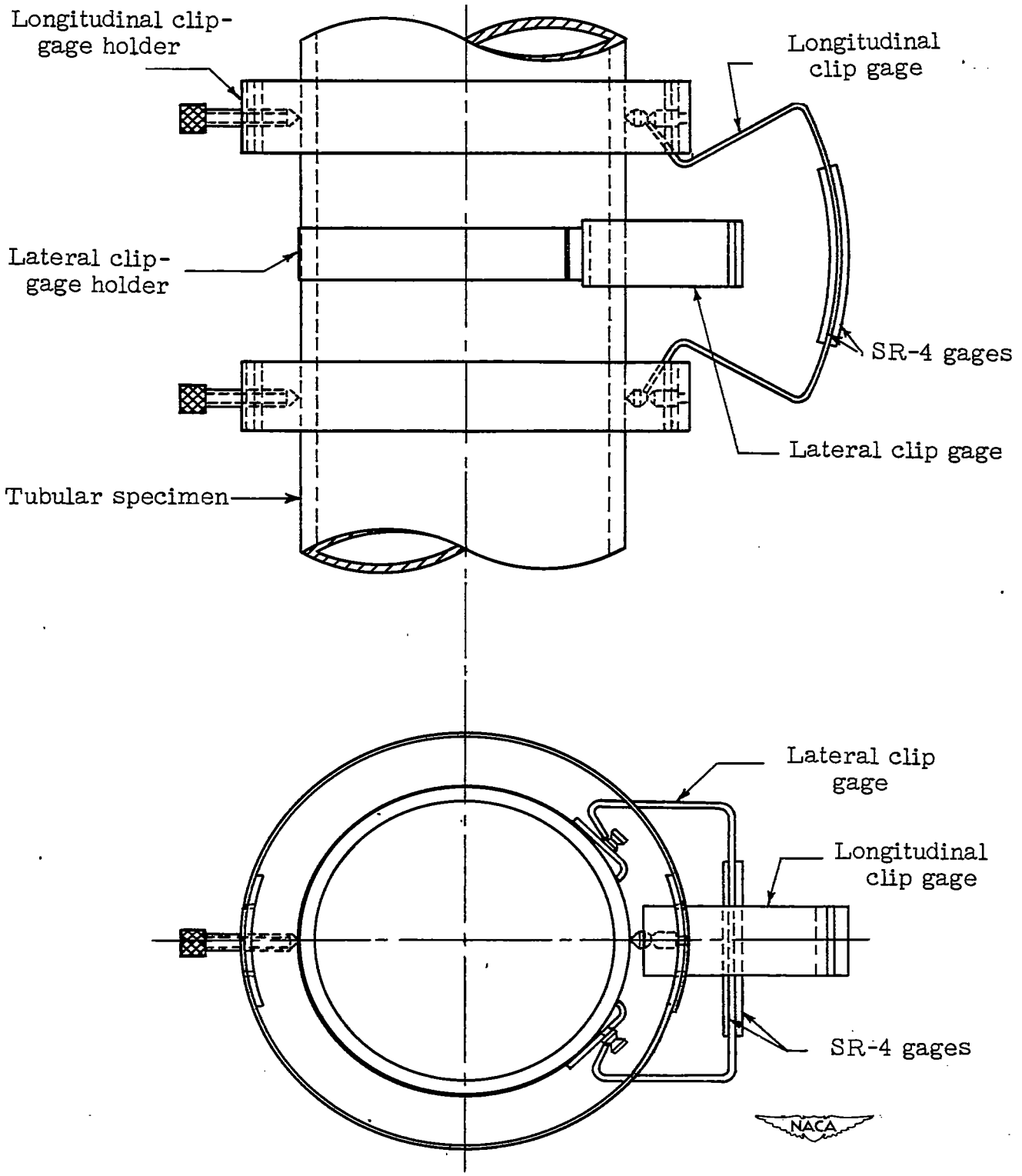

Figure 14.- Clip gages for measurement of plastic strains.

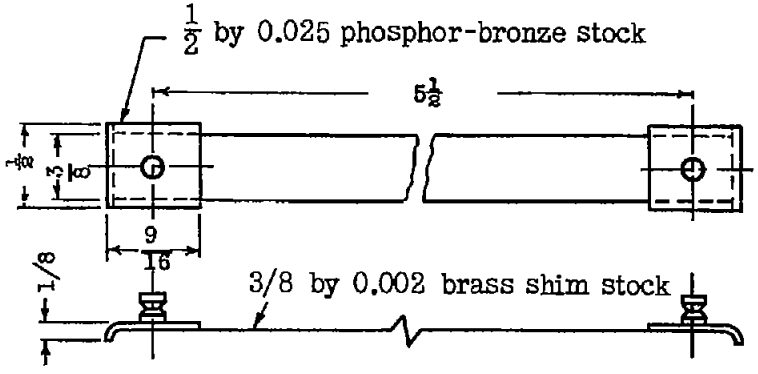

(a) Lateral clip-gage holder.

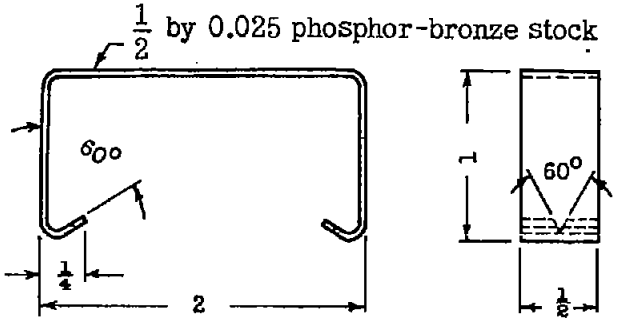

(b) Lateral clip gage.

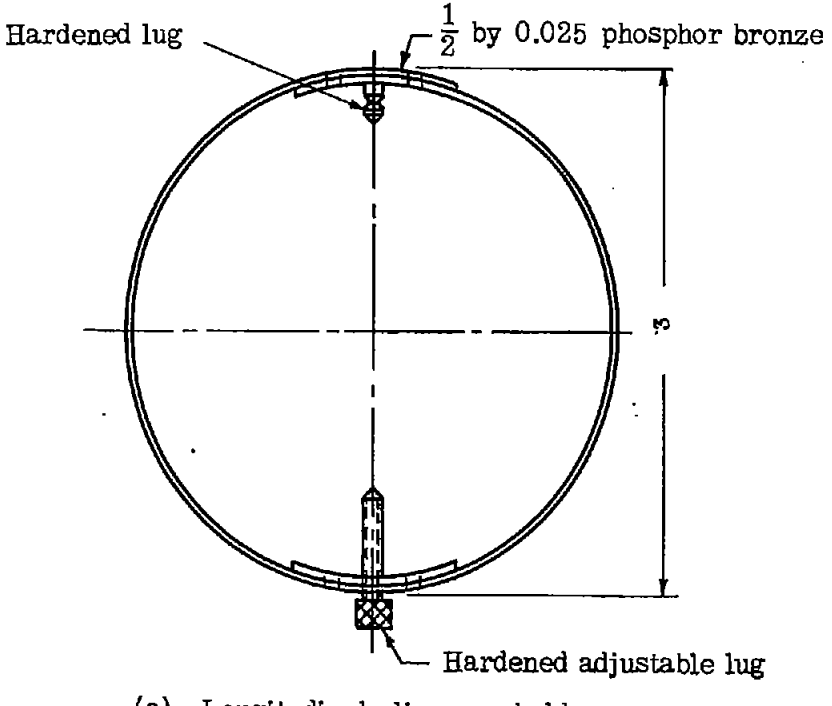

(c) Longitudinal clip-gage holder.

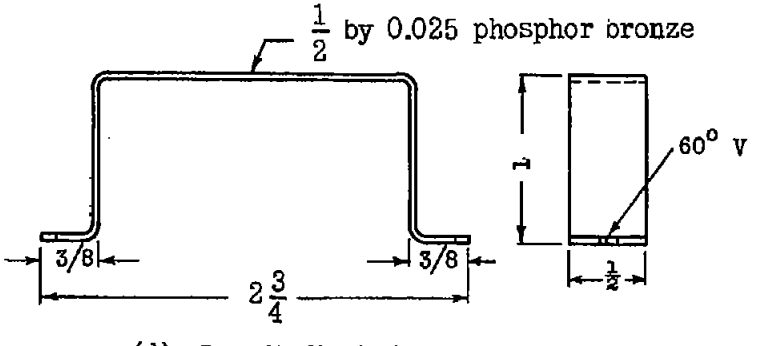

(d) Longitudinal clip gage.

Figure 15.- Longitudinal and lateral strain-measuring devices. All measurements are in inches.

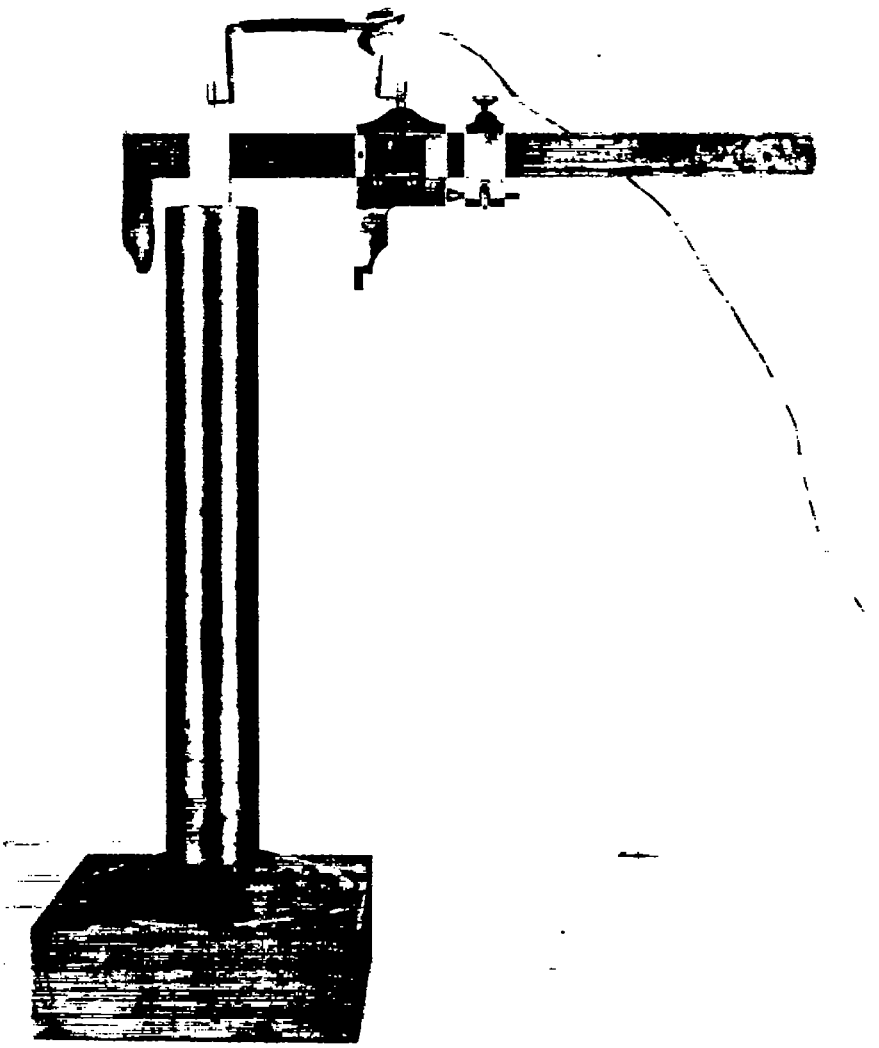

Figure 16.- Vernier device for calibrating longitudinal clip gages.

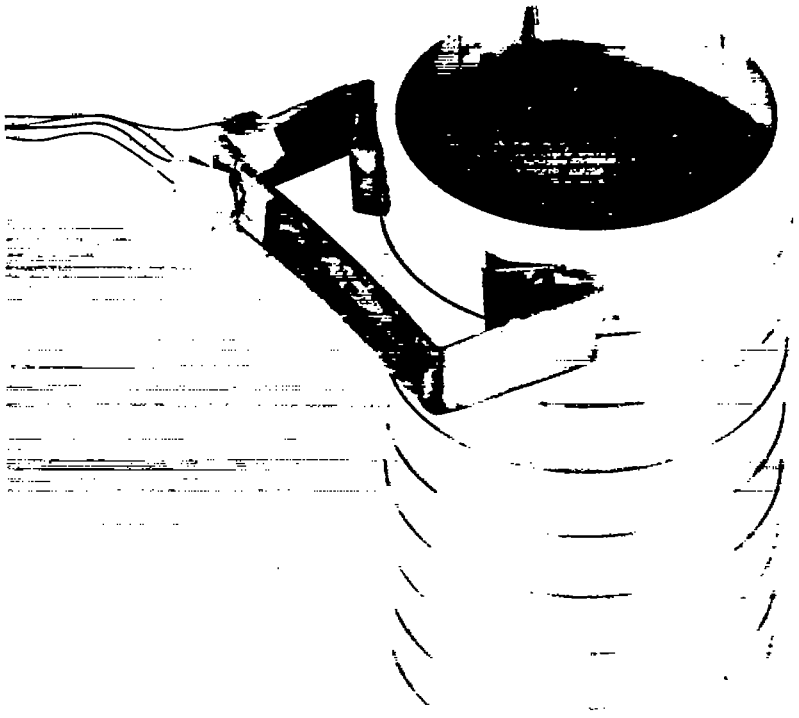

Figure 17.- Stepped-tube device for calibrating lateral clip gages.

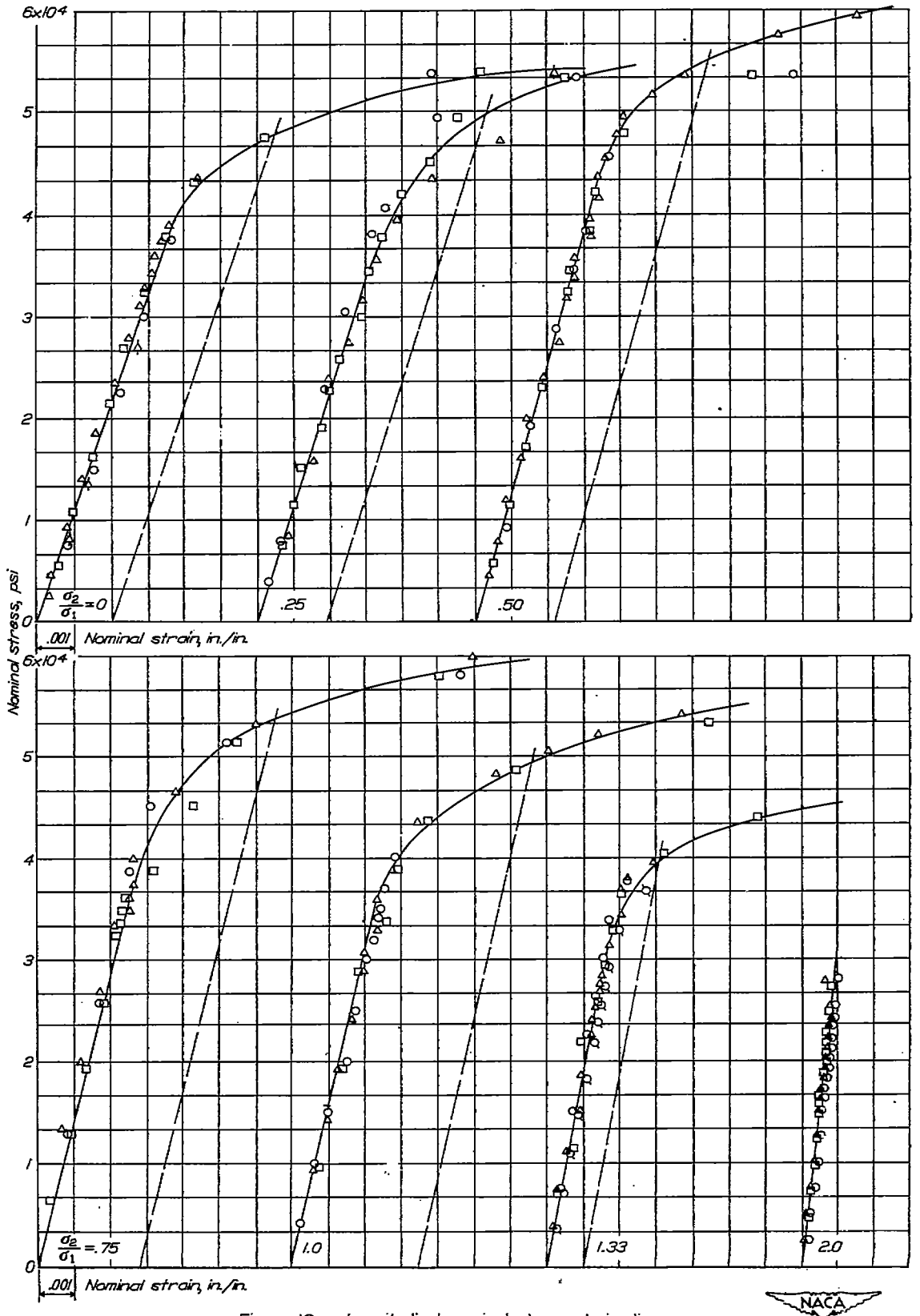

Figure 18.- Longitudinal nominal stress-strain diagrams.

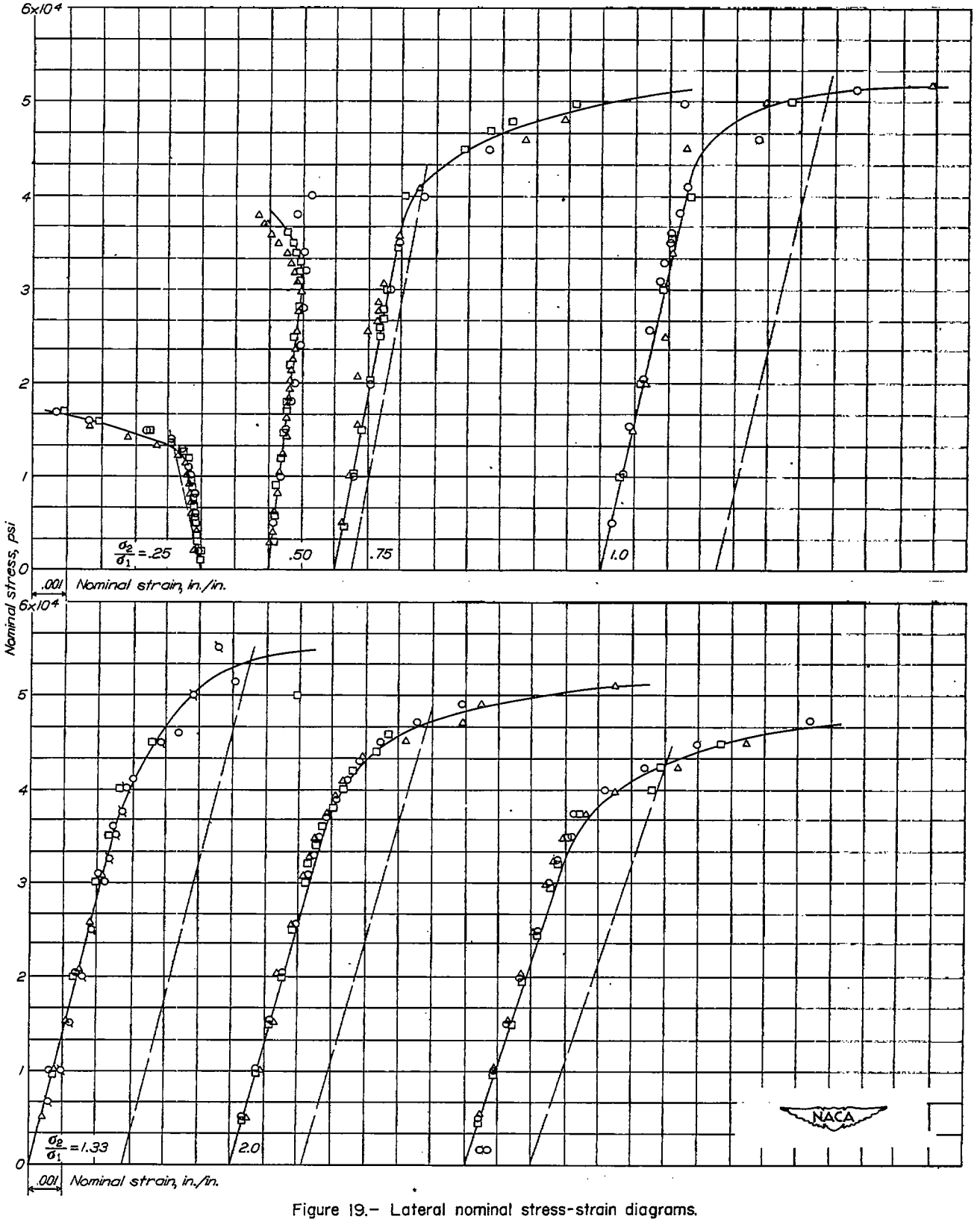

Figure 19.– Lateral nominal stress-strain diagrams.

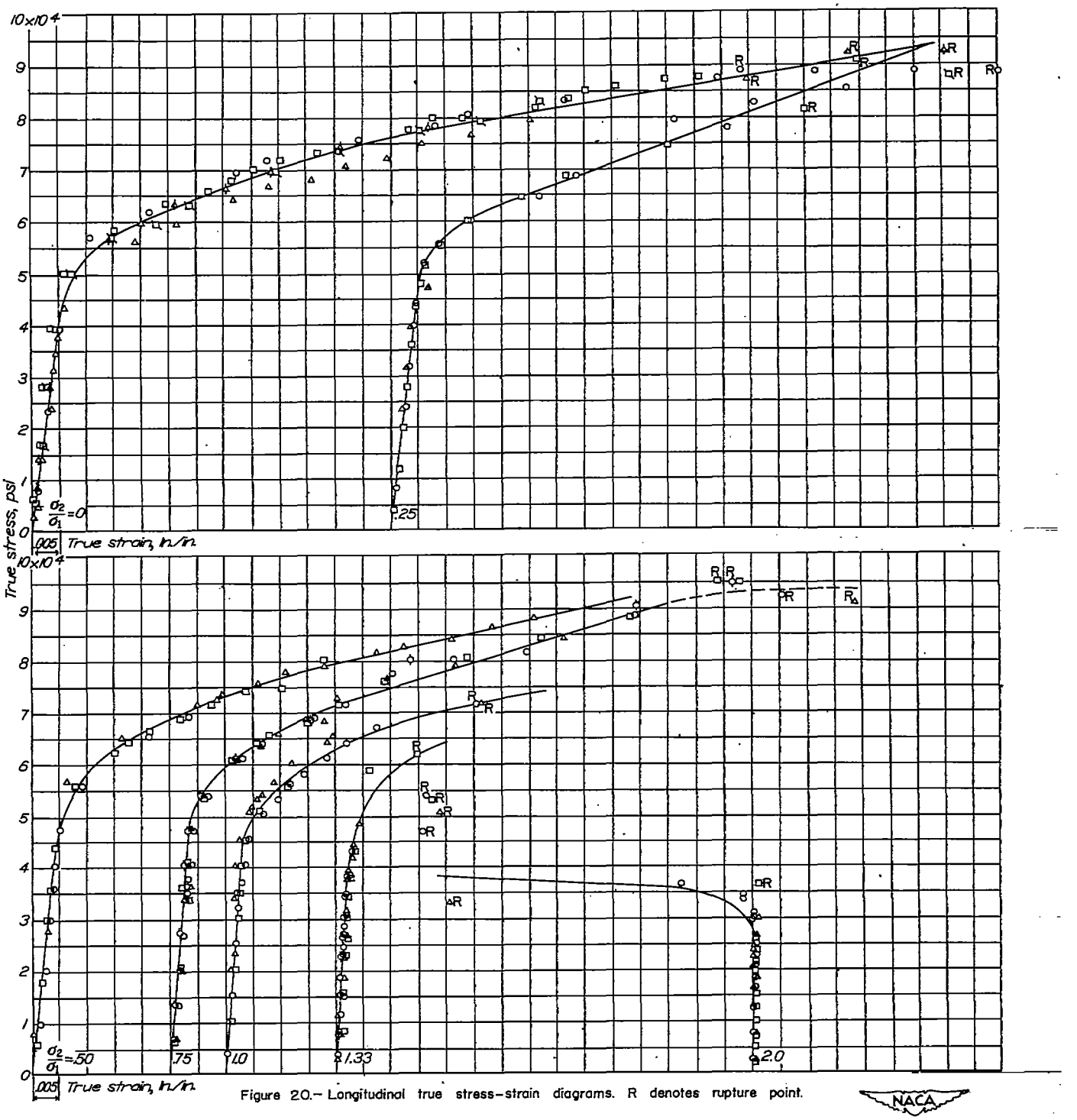

Figure 20.- Longitudinal true stress-strain diagrams. R denotes rupture point.

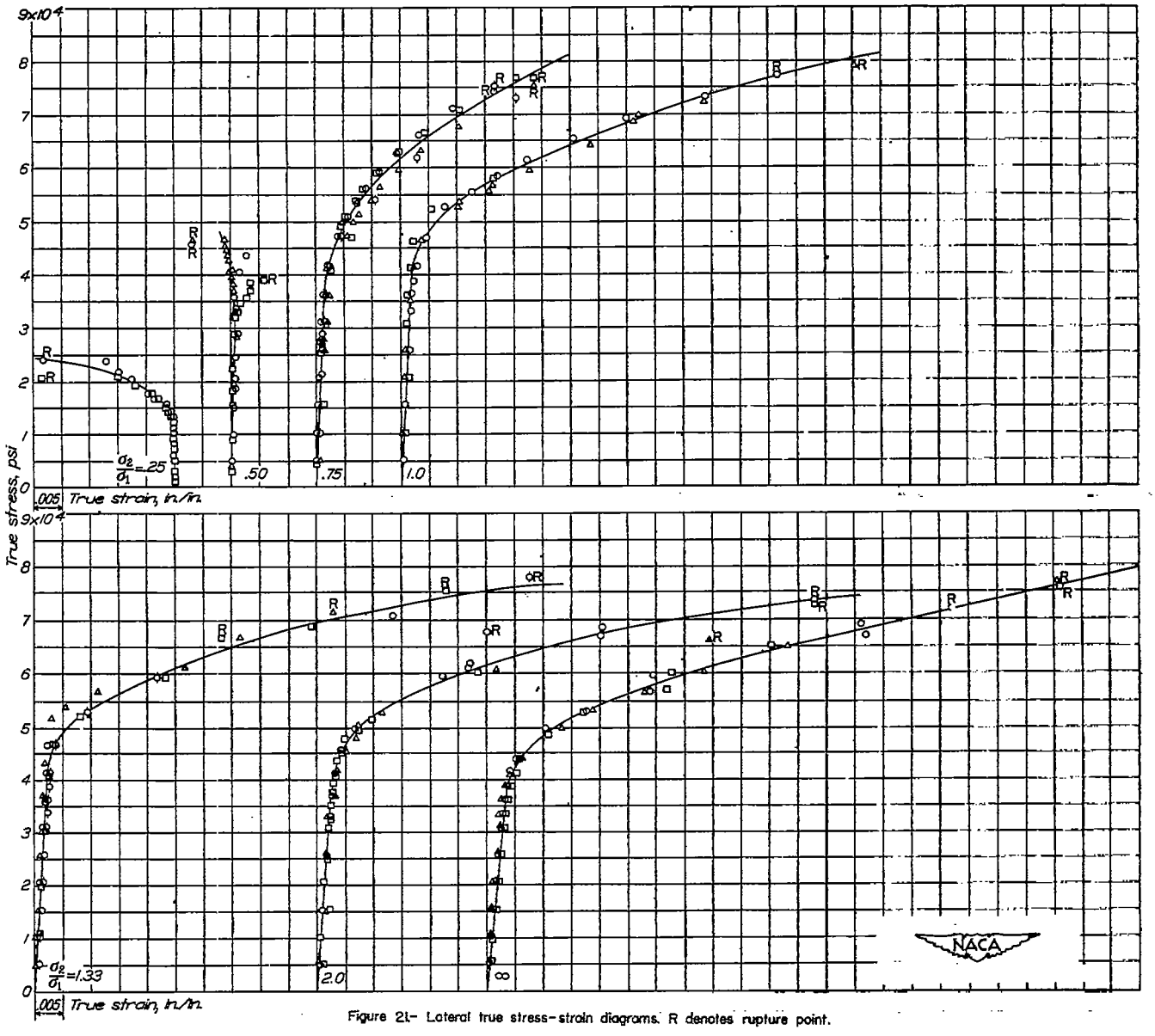

Figure 21- Lateral true stress-strain diagrams. R denotes rupture point.

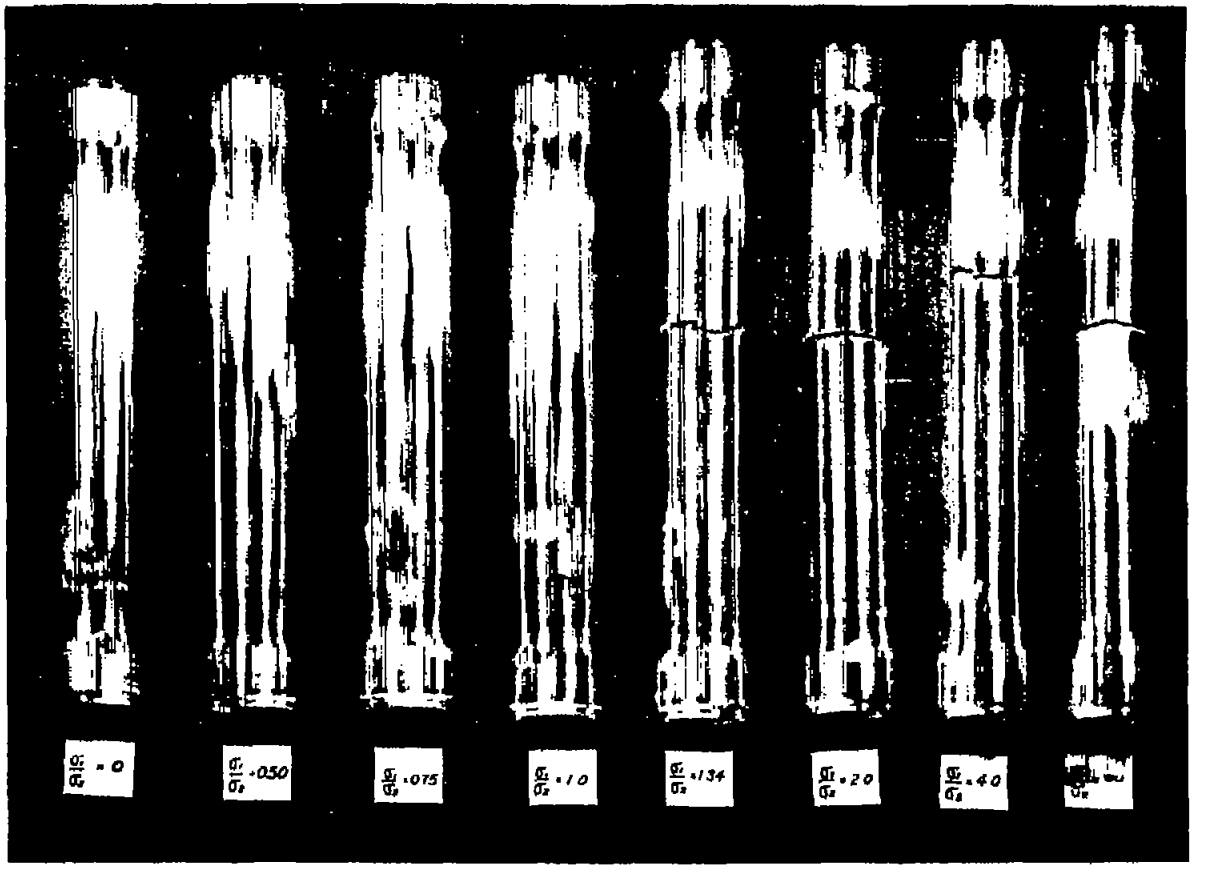

Figure 22.- Typical types of fracture for various stress ratios.

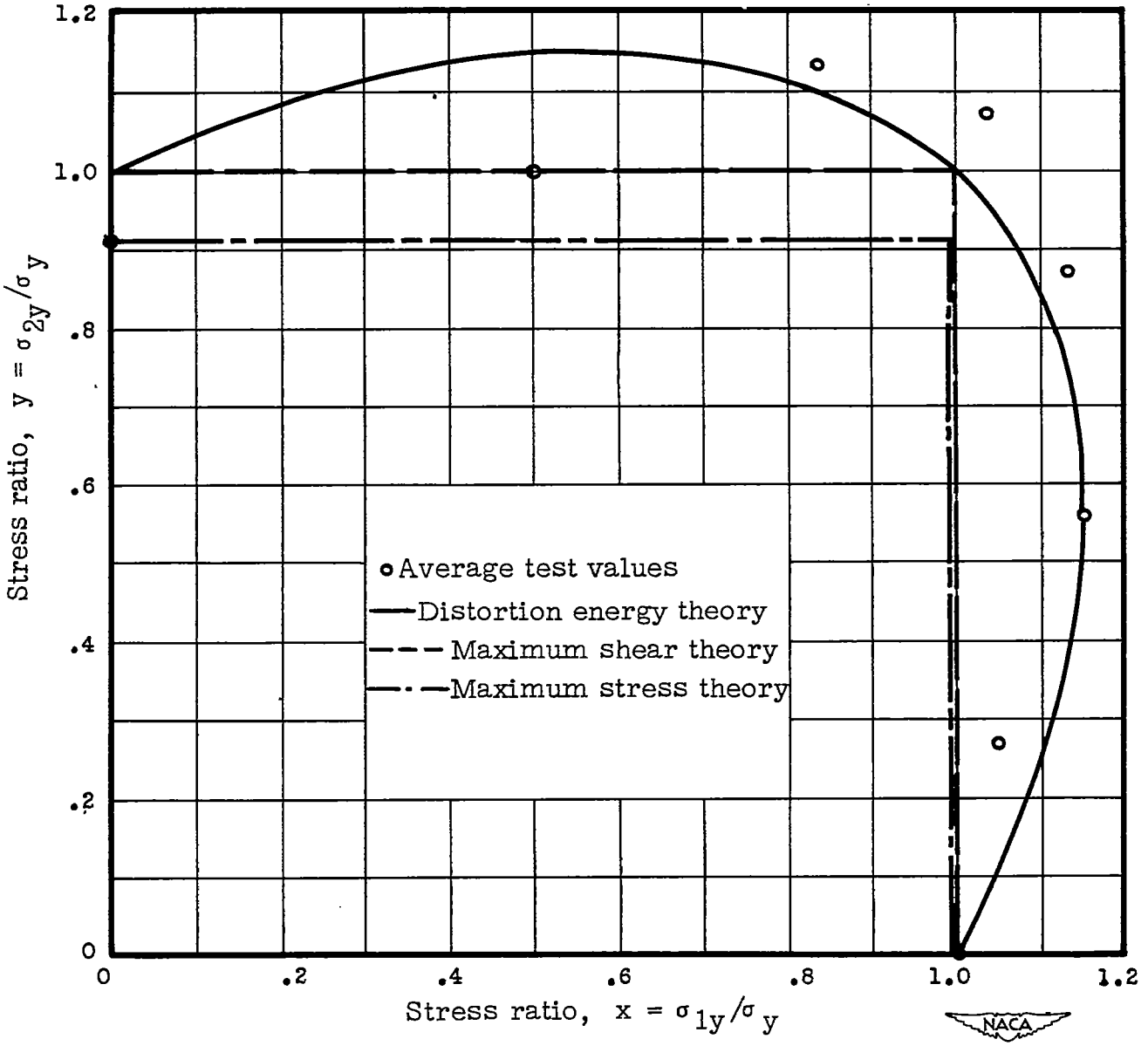

(a) Comparison of yield strengths with theories of failure.

Figure 23.- Comparison of test results with theories.

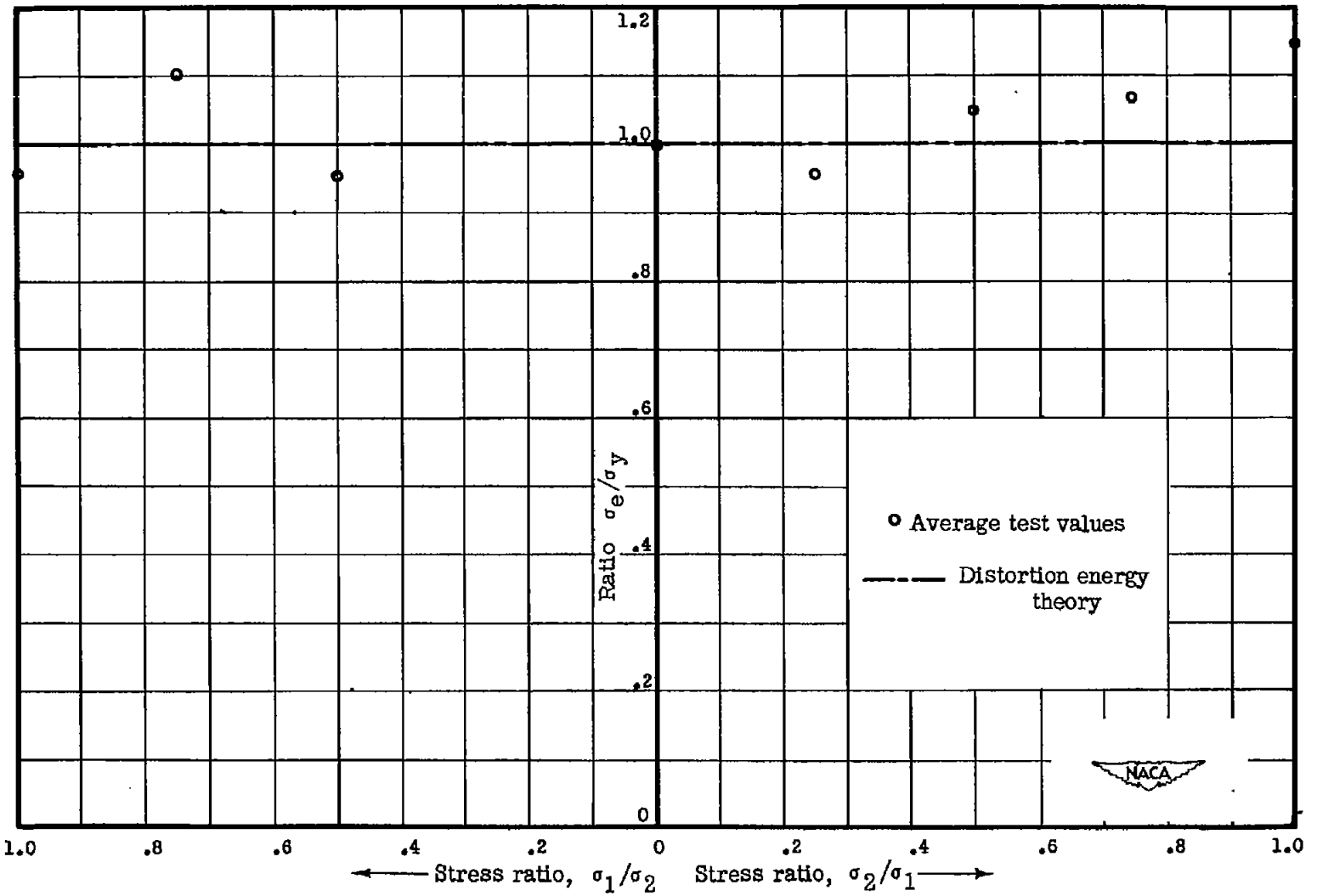

(b) Comparison of test results with distortion energy theory including effect of radial stress.

Figure 23.- Concluded.

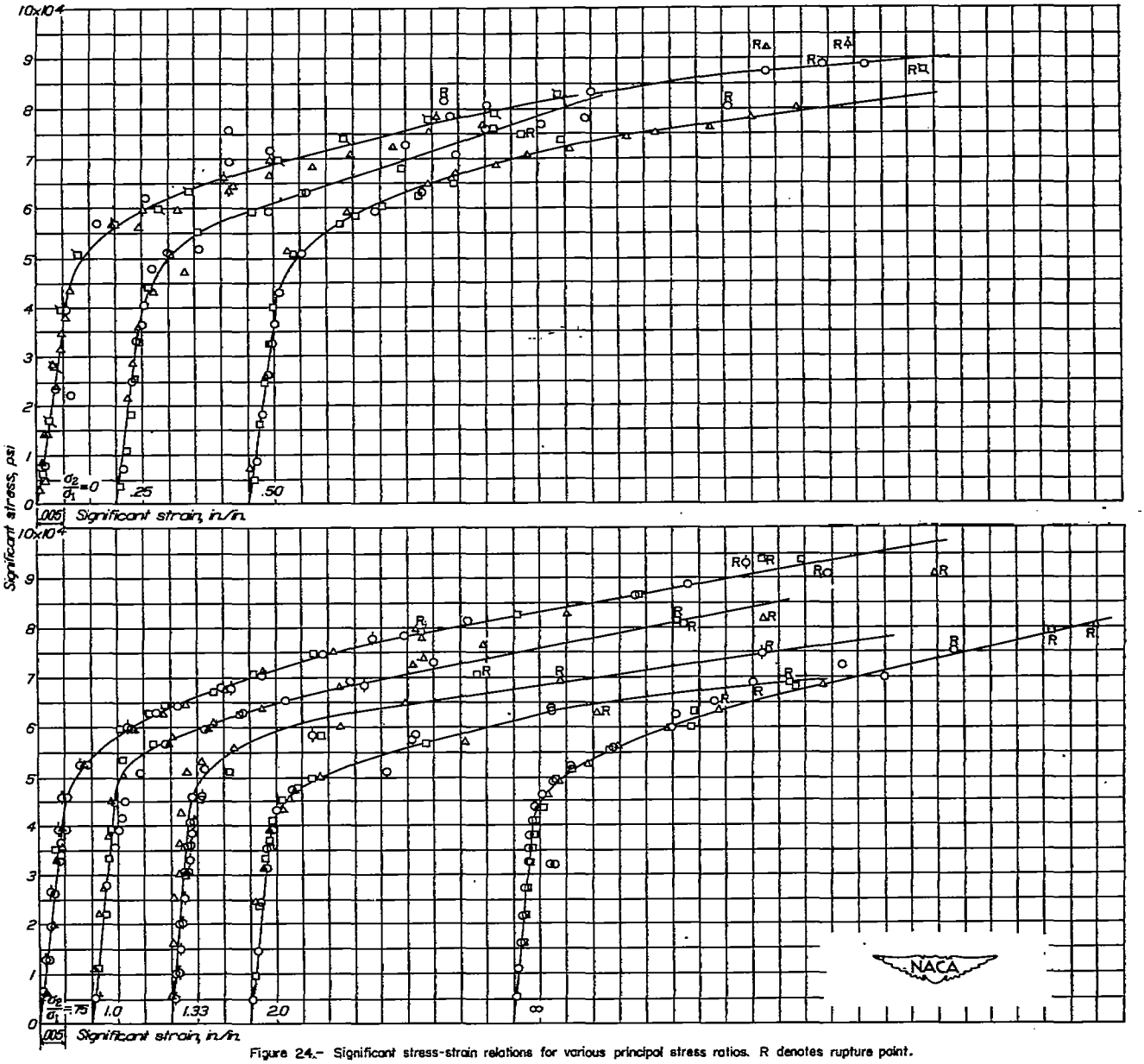

Figure 24.- Significant stress-strain relations for various principal stress ratios. R denotes rupture point.

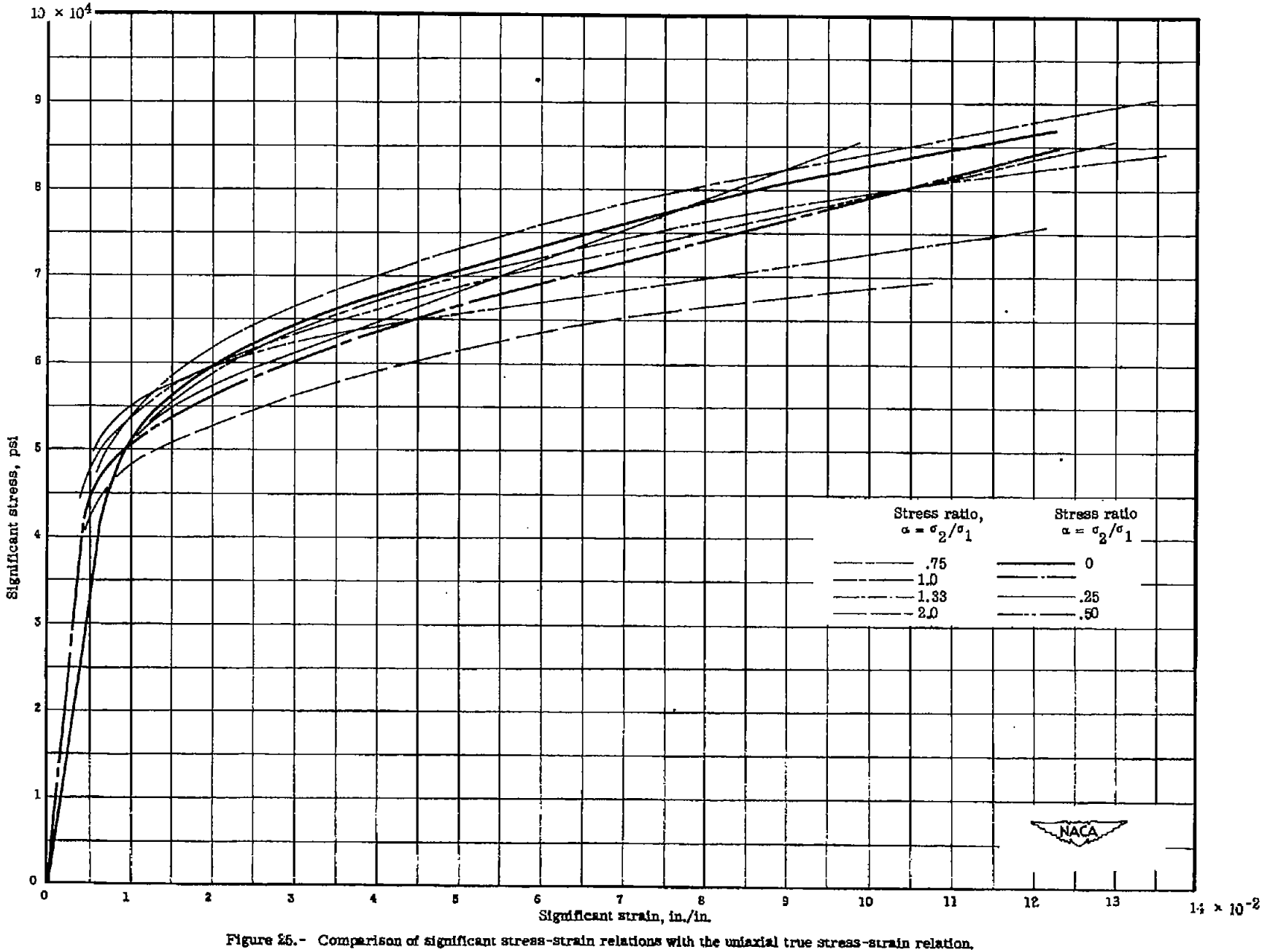

Figure 25.- Comparison of significant stress-strain relations with the uniaxial true stress-strain relation.

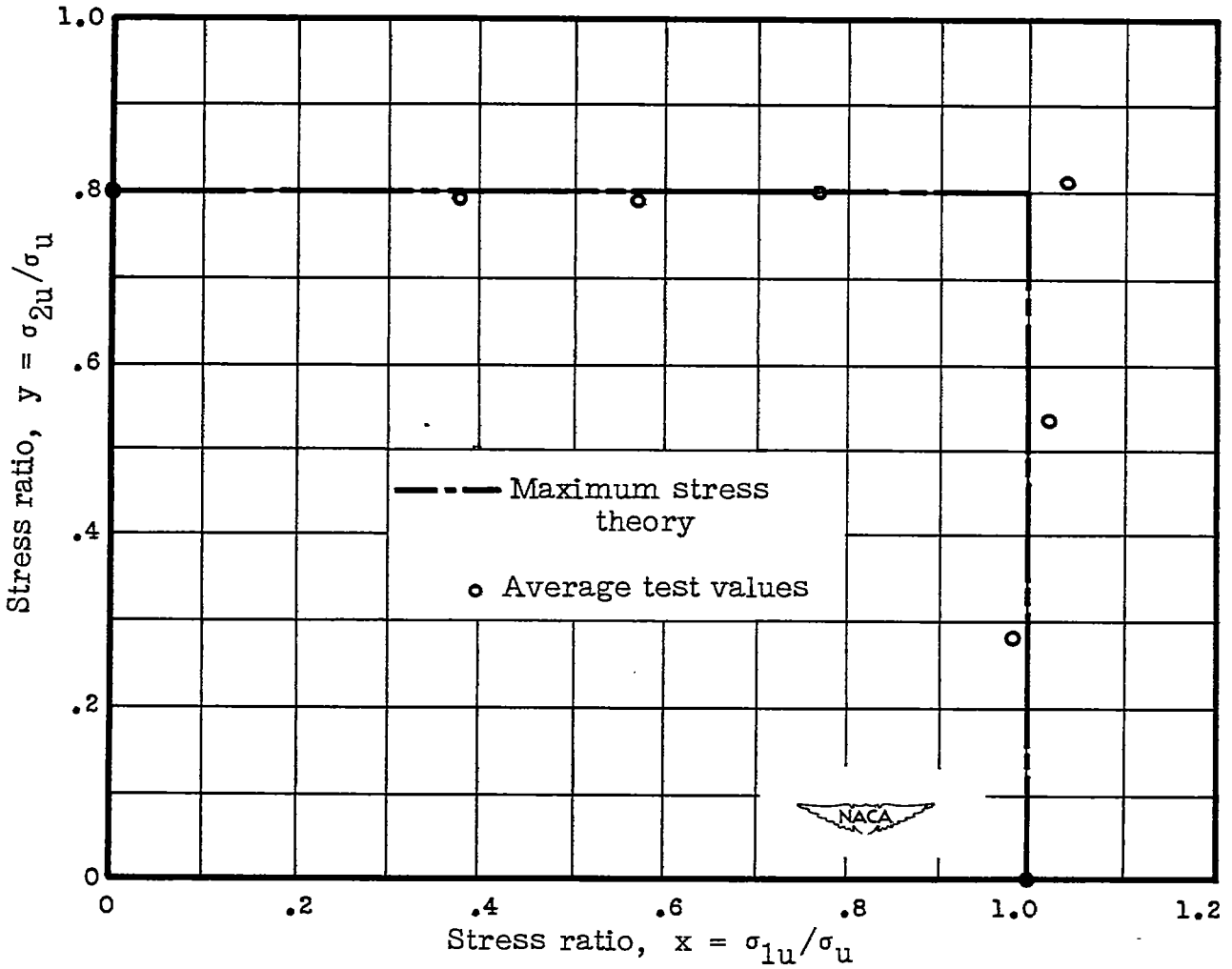

Figure 26.- Comparison of nominal biaxial ultimate strengths with values from maximum stress theory. Stress σ_u is nominal ultimate tensile stress in longitudinal direction.

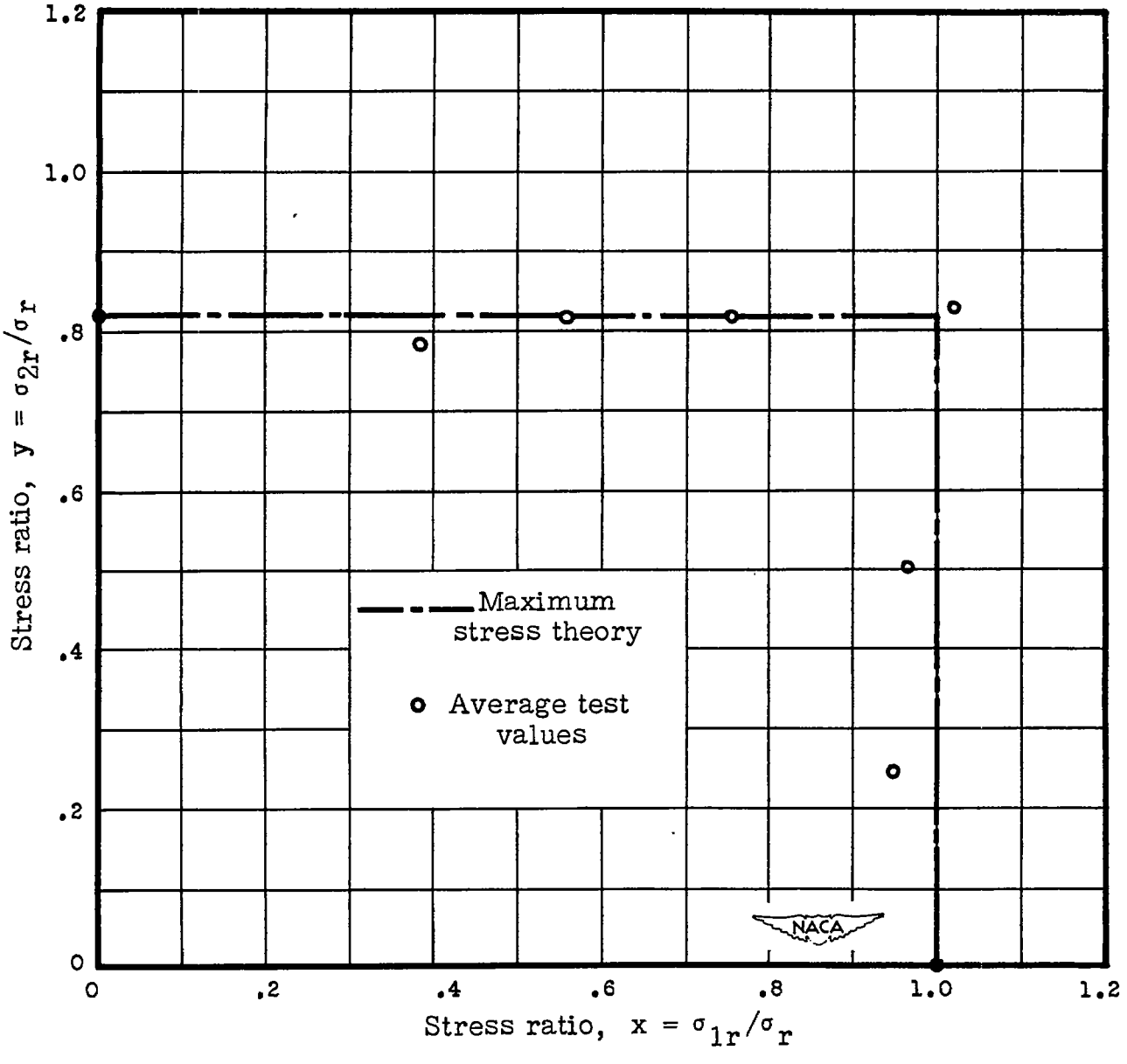

Figure 27.- Comparison of true biaxial fracture stresses with values from maximum stress theory.

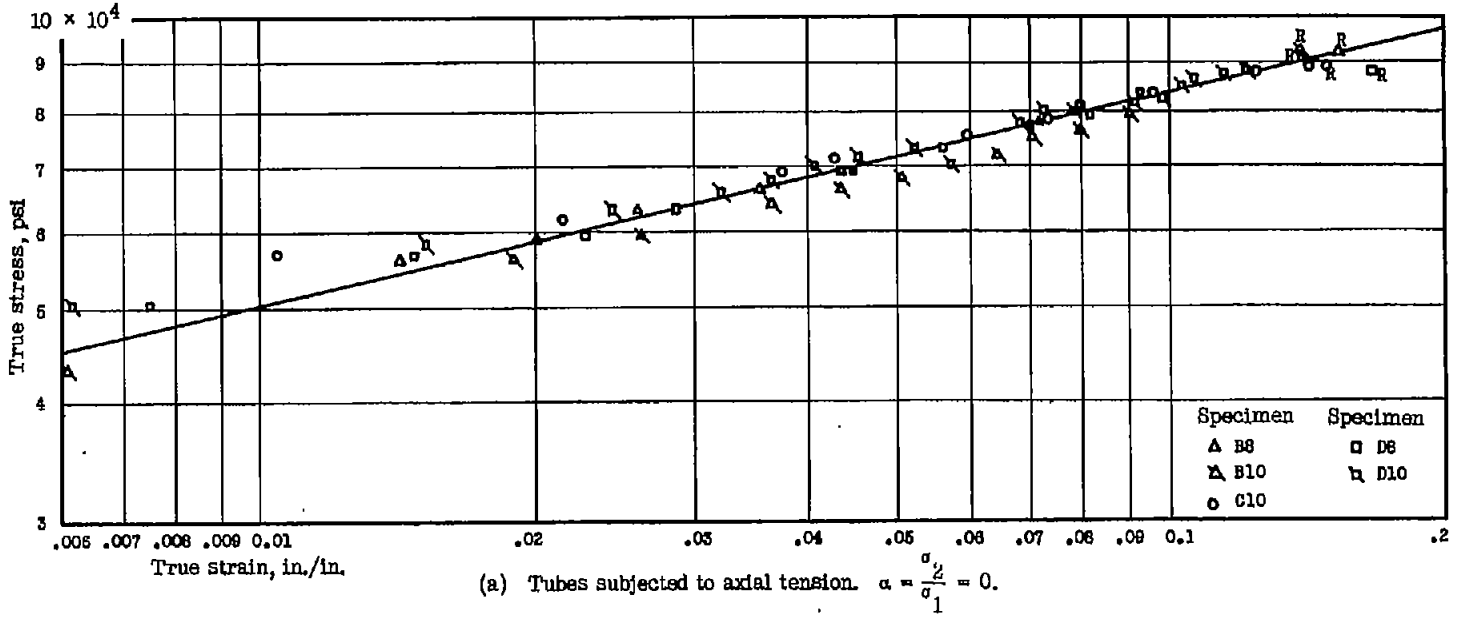

(a) Tubes subjected to axial tension. $\alpha = \frac{\sigma_2}{\sigma_1} = 0$.

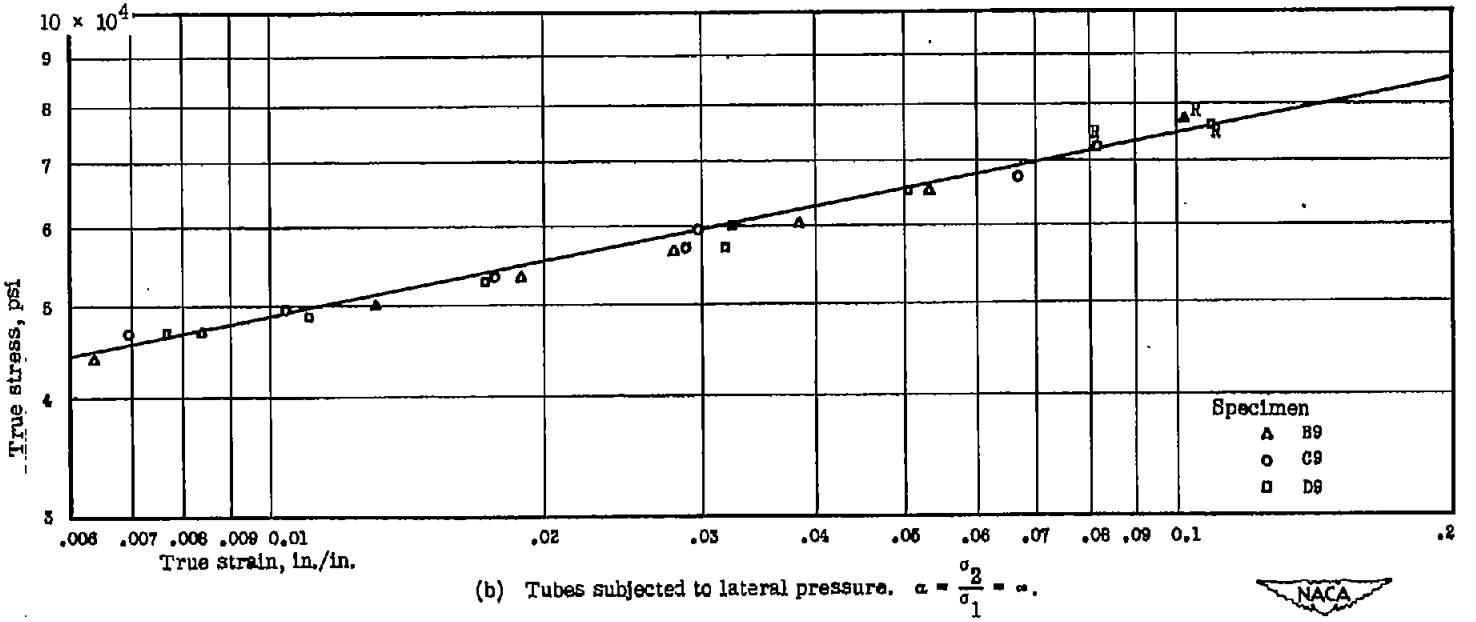

(b) Tubes subjected to lateral pressure. $\alpha = \frac{\sigma_2}{\sigma_1} = \infty$.

Figure 28.- True stress-strain relations for tension tests on tubes.

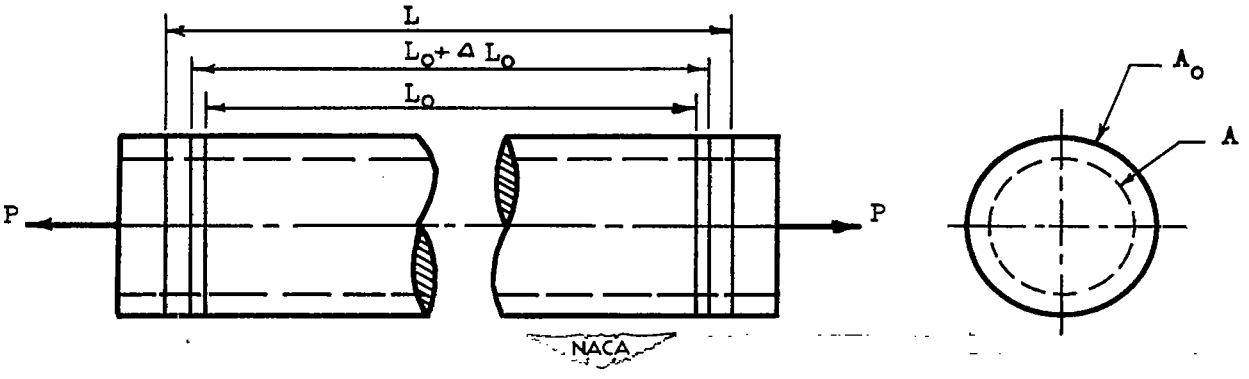

Figure 29.- Simple tension member.

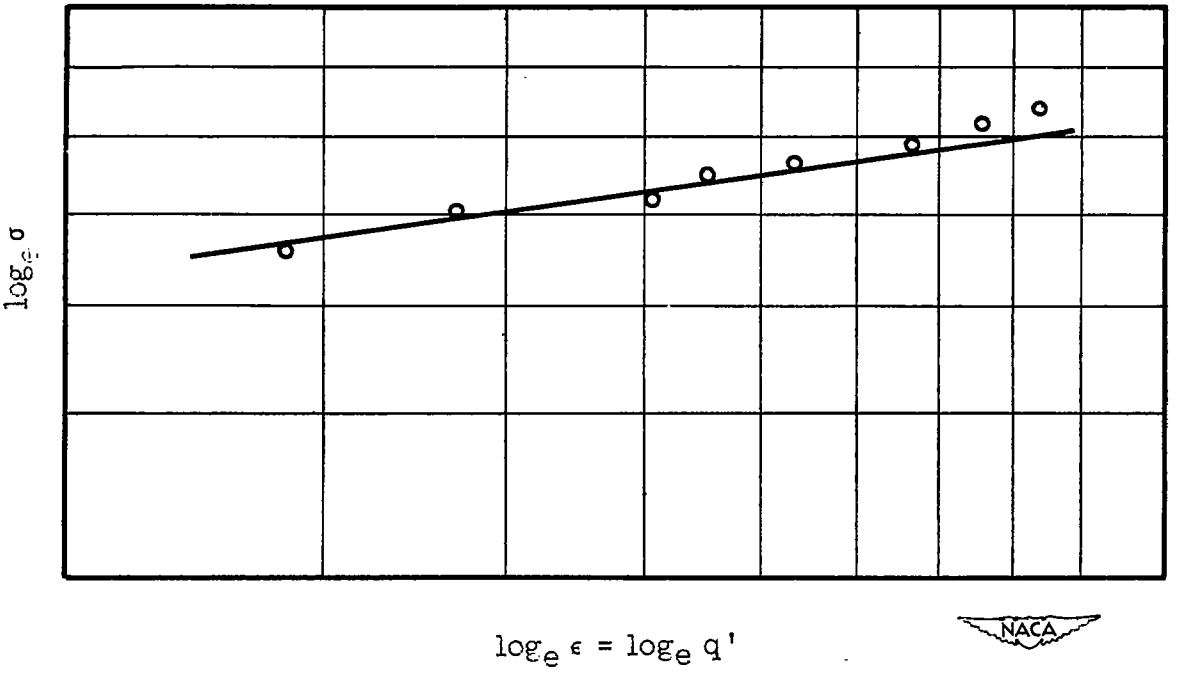

Figure 30.- Tension true stress-strain relation.

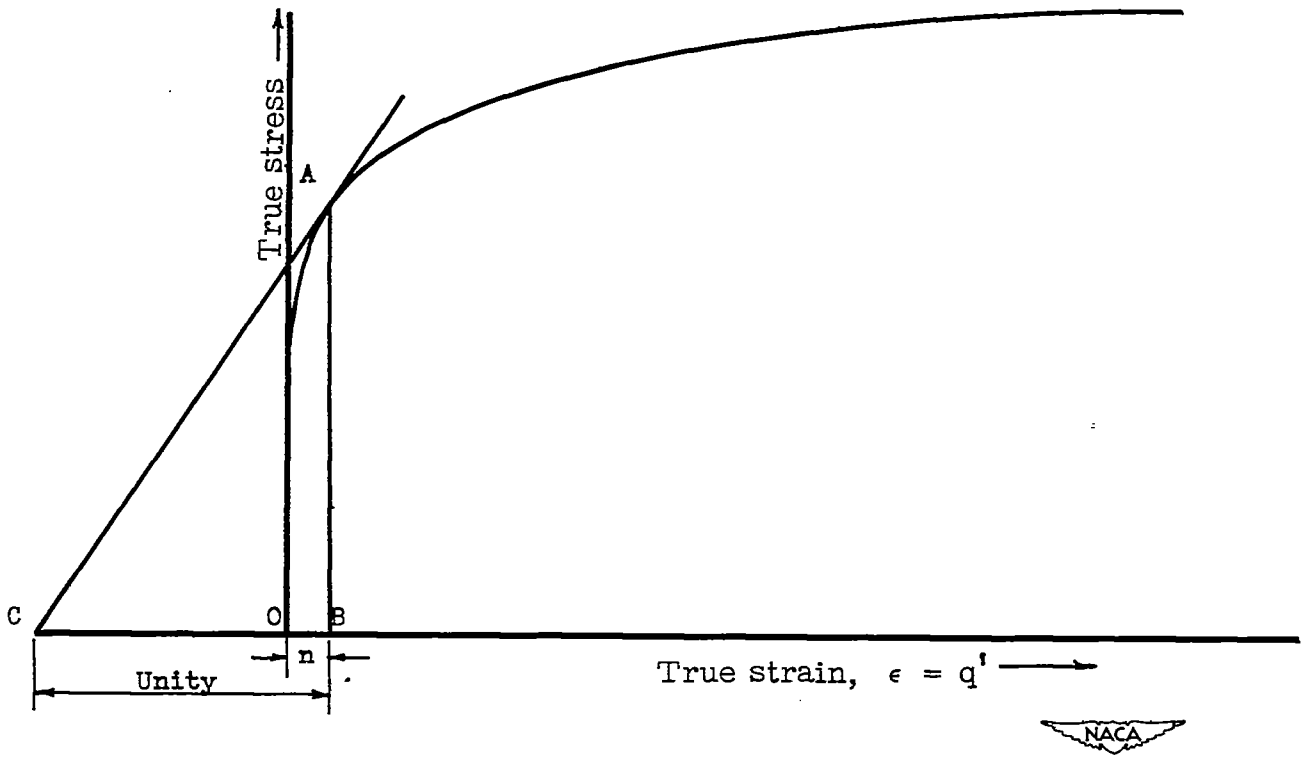

Figure 31.- Tension true stress-strain relation.

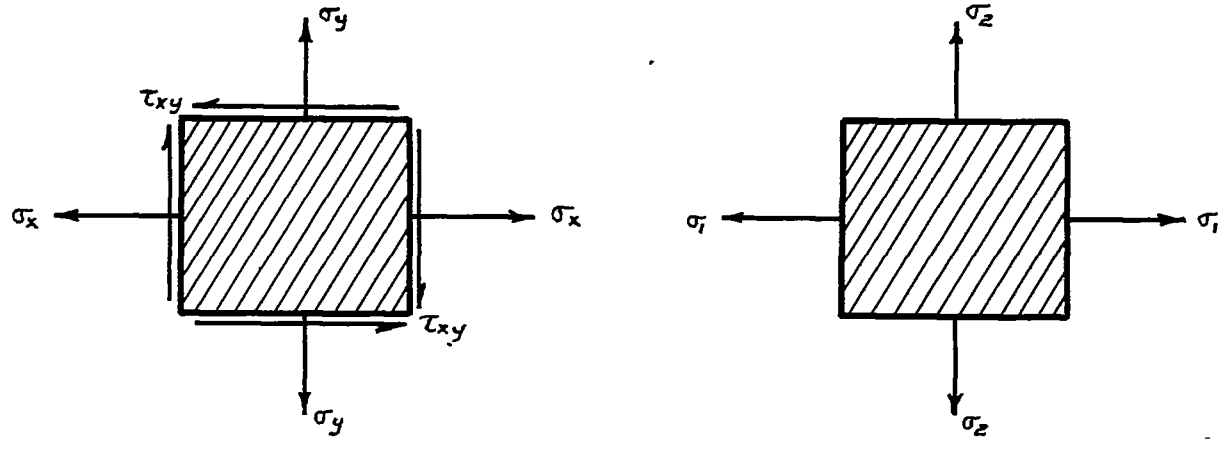

(a) Biaxial tension and shear. (b) Biaxial tension.

Figure 32.- Elements subjected to combined stresses.

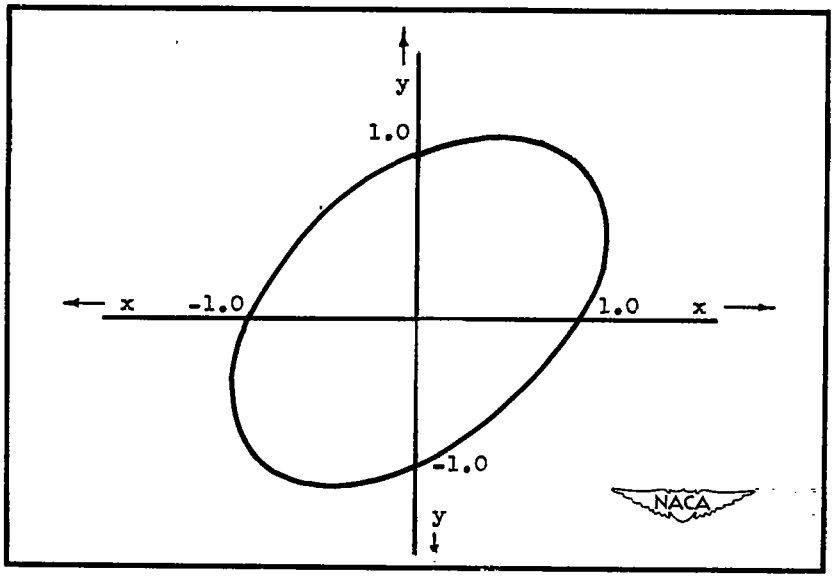

Figure 33.- Distortion energy theory of failure for yielding.

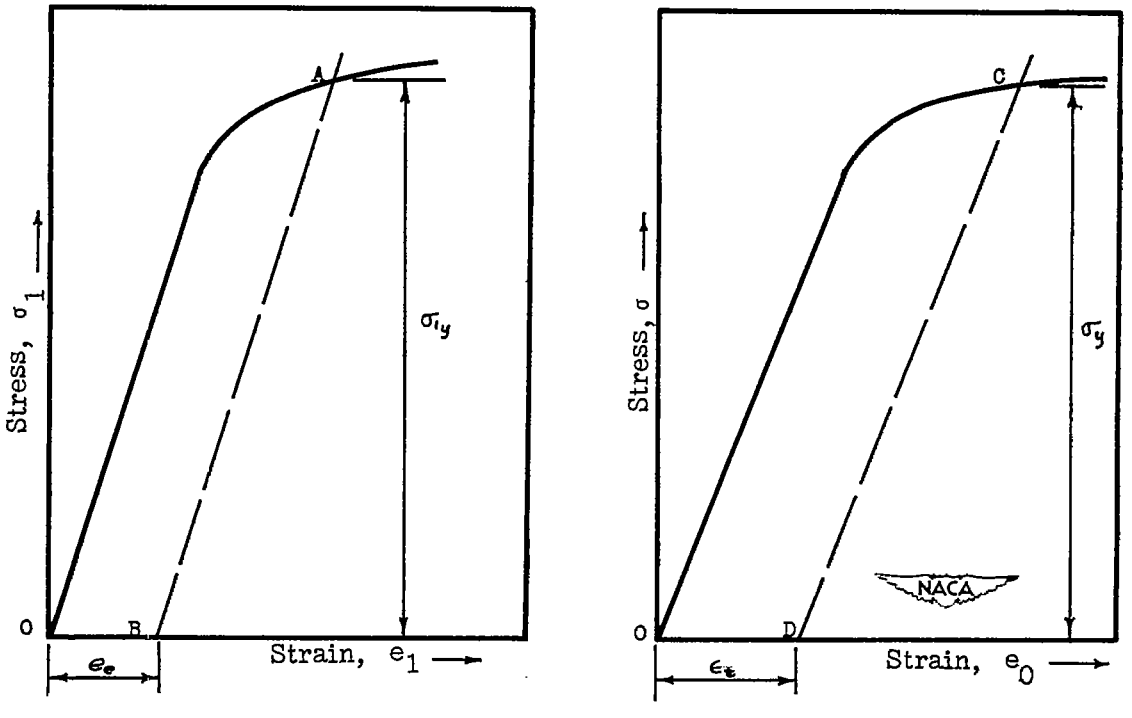

(a) Combined stresses. (b) Simple tension.

Figure 34.- Elastic stress-strain diagrams.

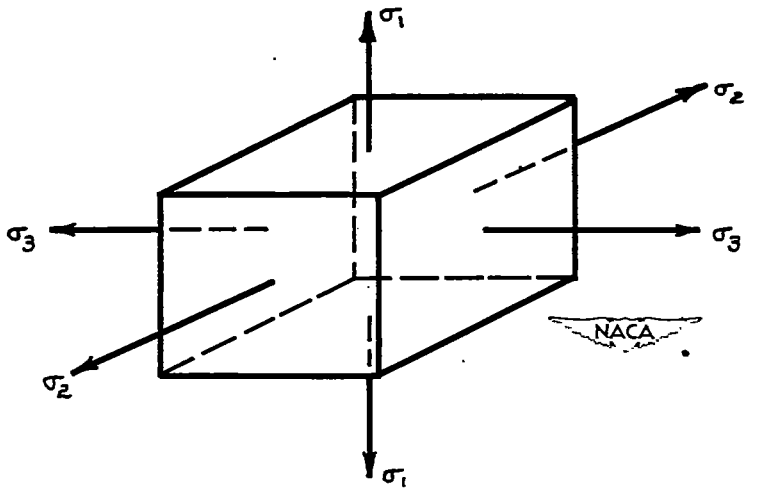

Figure 35.- Element subjected to triaxial stresses.

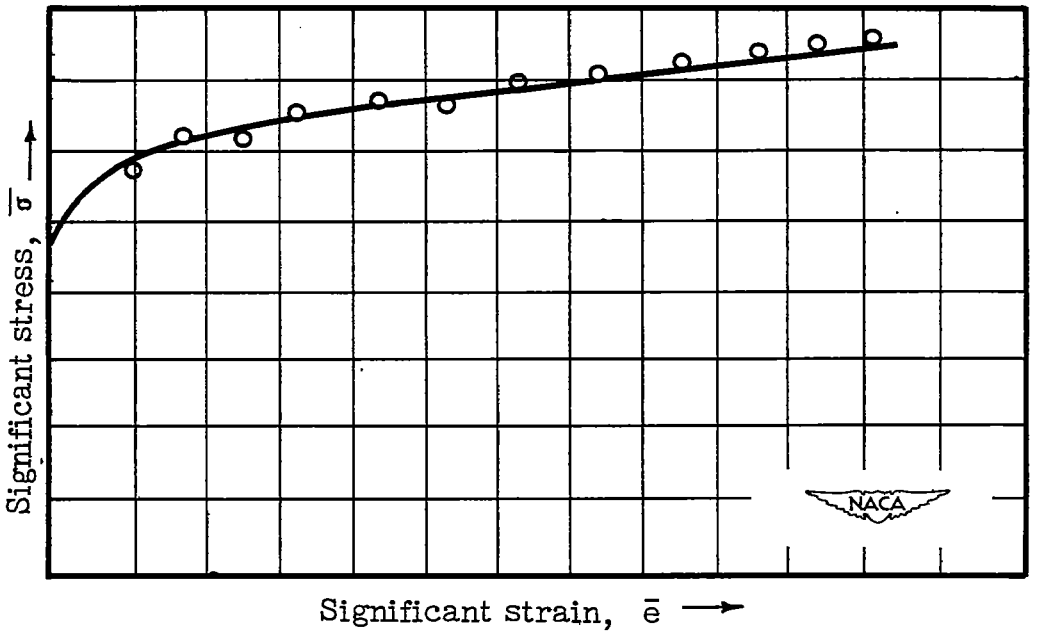

Figure 36.- Significant stress-strain relation.

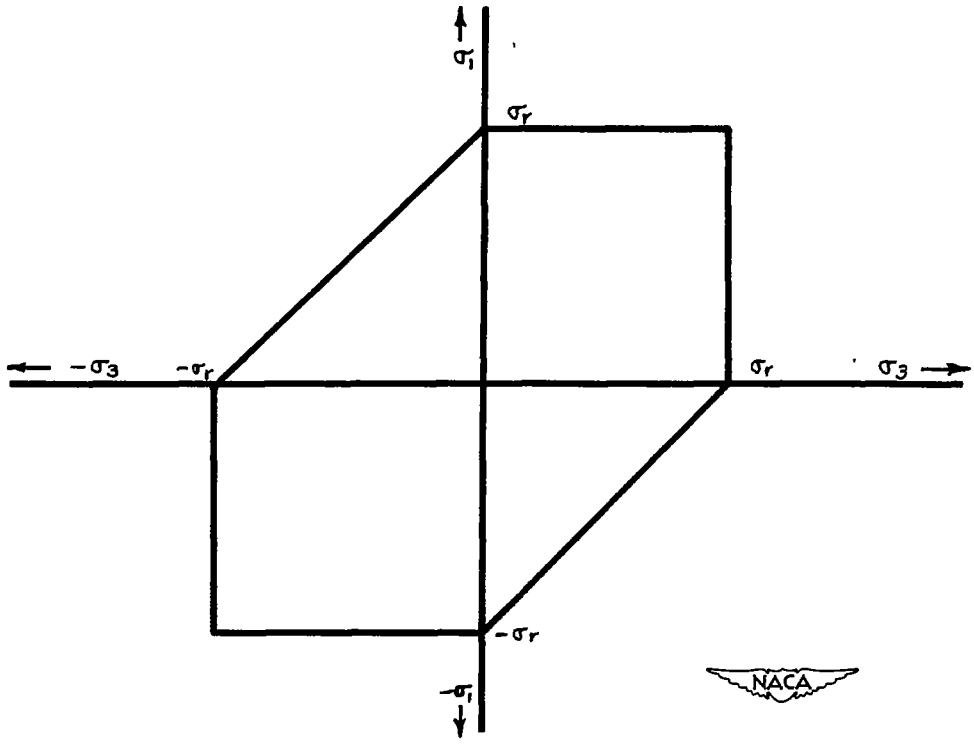

Figure 37.- Shear theory of failure for rupture.

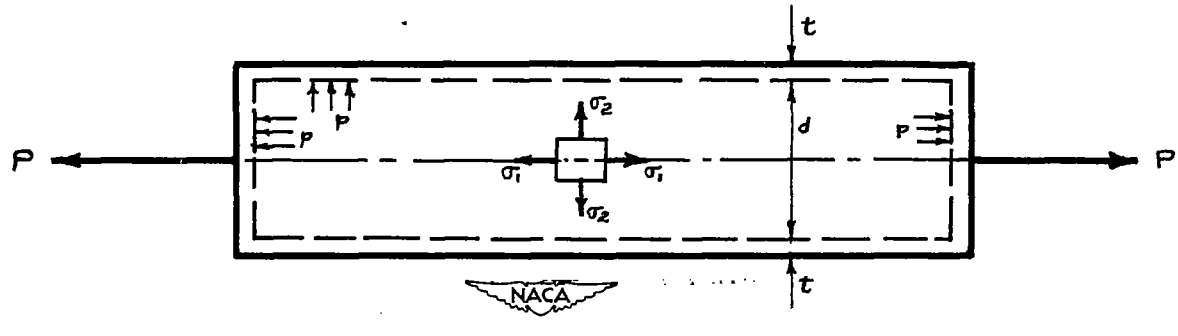

Figure 38.- Tubular specimen subjected to internal pressure and axial load.